Actin, microtubules, and vimentin intermediate filaments cooperate for elongation of invadopodia

Marie Schoumacher,[1,2] Robert D. Goldman,[3] Daniel Louvard,[1,2] and Danijela M. Vignjevic[1,2]

[1]Unité Mixte de Recherche 144, Centre National de la Recherche Scientifique, [2]Institut Curie, 75248 Paris, Cedex 05, France
[3]Feinberg School of Medicine, Northwestern University, Chicago, IL 60611

Invasive cancer cells are believed to breach the basement membrane (BM) using specialized protrusions called invadopodia. We found that the crossing of a native BM is a three-stage process: invadopodia indeed form and perforate the BM, elongate into mature invadopodia, and then guide the cell toward the stromal compartment. We studied the remodeling of cytoskeleton networks during invadopodia formation and elongation using ultrastructural analysis, spatial distribution of molecular markers, and RNA interference silencing of protein expression. We show that formation of invadopodia requires only the actin cytoskeleton and filopodia- and lamellipodia-associated proteins. In contrast, elongation of invadopodia is mostly dependent on filopodial actin machinery. Moreover, intact microtubules and vimentin intermediate filament networks are required for further growth. We propose that invadopodia form by assembly of dendritic/diagonal and bundled actin networks and then mature by elongation of actin bundles, followed by the entry of microtubules and vimentin filaments. These findings provide a link between the epithelial to mesenchymal transition and BM transmigration.

Introduction

The formation of metastases in distant organs is a critical step in cancer progression and is the major cause of mortality. To escape from the primary tumor and invade adjacent tissues, cancer cells must degrade the basement membrane (BM) that separates the epithelial and stromal compartments (Thiery, 2002). The degradation of the BM is performed by matrix metalloproteinases (MMPs). In cell culture assays, MMPs accumulate in fingerlike membrane protrusions, termed invadopodia, that form on the ventral surface of cancer cells (Chen, 1989; Linder, 2007; Poincloux et al., 2009). Invadopodia are actin-rich structures, and the actin polymerization machinery is critical for both their formation and function (Buccione et al., 2004; Lorenz et al., 2004; Yamaguchi et al., 2005; Artym et al., 2006; Baldassarre et al., 2006; Bowden et al., 2006; Weaver, 2006; Clark et al., 2007; Philippar et al., 2008; Sakurai-Yageta et al., 2008; Lizárraga et al., 2009).

On a two-dimensional substratum, protrusion of the cell leading edge is driven by polymerization of actin within two structures, filopodia and lamellipodia. In lamellipodia, actin organizes into a mesh of unbundled filaments, often described as dendritic or diagonal networks (Svitkina and Borisy, 1999; Koestler et al., 2008), whereas in filopodia, actin filaments organize into parallel bundles (Gupton and Gertler, 2007; Mattila and Lappalainen, 2008). These two different types of organization rely on the action of specific actin-organizing proteins. In lamellipodia, the formin mDia2 is targeted to the plasma membrane where it may nucleate mother filaments, which then serve as a base for Arp2/3-dependent nucleation of actin branches (Yang et al., 2007), which are further stabilized by cortactin (Higgs and Pollard, 2001; Weaver et al., 2001). At the same time, any unnecessary growing barbed ends are capped by capping protein (Wear and Cooper, 2004). If barbed ends are protected from capping by mDia2 itself (Yang et al., 2007) or VASP (vasodilator-stimulated phosphoprotein; Bear et al., 2002; Trichet et al., 2008), actin filaments continue to elongate persistently and gradually converge to form filopodia. Behind the leading edge of the lamellipodium, longer unbranched filaments are cross-linked by the actin-binding protein (ABP) α-actinin, whereas in filopodia, long parallel actin filaments are

Correspondence to Marie Schoumacher: marie.schoumacher@curie.fr; or Danijela M. Vignjevic: danijela.vignjevic@curie.fr

Abbreviations used in this paper: ABP, actin-binding protein; BM, basement membrane; HGF, hepatocyte growth factor; MMP, matrix metalloproteinase; tyr-tubulin, tyrosinated tubulin; VASP, vasodilator-stimulated phosphoprotein.

The Rockefeller University Press $30.00
J. Cell Biol.
www.jcb.org/cgi/doi/10.1083/jcb.200909113

tightly bundled by fascin and to some degree T-fimbrin (Svitkina et al., 2003; Vignjevic et al., 2006). Molecular traffic and signaling along filopodial shafts are mediated by the molecular motor myosinX (Sousa and Cheney, 2005; Pi et al., 2007; Mattila and Lappalainen, 2008).

These two types of actin organization have distinct roles in the cell: the dendritic network in a lamellipodium produces a force that is sufficient to drive membrane protrusion and cell crawling on a planar substrate, whereas the tight actin bundle in a filopodium produces the required stiffness to form a rodlike projection that is believed to be used by the cell to explore the environment and infiltrate between small gaps. Therefore, actin bundling and the subsequent formation of fingerlike protrusions could be a general mechanism for penetration of the substratum. For example, invasive cancer cells could exploit actin dynamics by using actin bundles to form invadopodia that penetrate the BM and invade the stroma (Vignjevic and Montagnac, 2008). In support of this hypothesis, fascin, an actin-bundling protein, is widely overexpressed in invasive cancers of different cellular origins (Hashimoto et al., 2005), demonstrating specific up-regulation at the invasive tumor front (Vignjevic et al., 2007). Invadopodia formation appears to depend both on proteins involved in the generation of a dendritic actin network such as Arp2/3 (Yamaguchi et al., 2005; Baldassarre et al., 2006) and cortactin (Artym et al., 2006; Bowden et al., 2006; Clark et al., 2007) and also on proteins involved in the generation of an unbranched actin network such as VASP (Philippar et al., 2008) and mDia2 (Lizárraga et al., 2009). Consequently, the regulation of actin organization in invadopodia remains a contentious issue. The majority of studies on invadopodia have focused on the actin cytoskeleton, with comparatively little research into the other two major cytoskeletal networks consisting of microtubules and intermediate filaments. Intact microtubules are known to be required for the function of invadopodia-related structures, podosomes, formed in monocytes and osteoclasts (Kopp et al., 2006; Linder, 2007), but they do not play a role in invadopodia formation (Kikuchi and Takahashi, 2008). A connection between microtubules and MMP trafficking in invadopodia may exist because the exocytosis of MMP-2 and -9 in melanoma cells is microtubule dependent (Schnaeker et al., 2004). There is also evidence supporting fimbrin-mediated interactions between actin and vimentin filaments in the formation of podosomes (Correia et al., 1999).

Studies into the formation and dynamics of invadopodia have been performed mostly on thin layers of ECM that have been coated directly onto glass (Weaver, 2006, 2008; Linder, 2007). These conditions do not accurately reflect the physiological environment because the extension of the invadopodia beyond the thin matrix layer is blocked by glass. Determining the organization and the role of the cytoskeleton during invasion is not feasible in these topologically restricted experimental conditions. Therefore, we have developed a new assay that more closely mimics the process of cancer cell invasion, permitting us to study the remodeling of the actin cytoskeleton during the formation and maturation of invadopodia. This assay has also enabled us to assess the role of other two cytoskeleton networks, microtubules and intermediate filaments, during the early stages of cancer cell invasion.

Results

The dissolution of the BM is a three-stage process

To visualize how invasive cancer cells pass through the BM to infiltrate the subjacent stroma, we isolated a native BM from the rat peritoneum as previously described (Hotary et al., 2006). In the absence of cancer cells, no holes were present in the BM, confirming that the membranes obtained during the isolation procedure were intact (Fig. 1 A). Next, we tested the ability of different types of cancer cells to penetrate the BM. The colon cancer cell line HT29 with poor metastatic potential was unable to degrade the BM even after 4 d of culture, confirming their incapacity to invade (Fig. 1 B). On the contrary, the metastatic breast cancer cells MDA-MB-231 and colon cancer cells HCT116 succeeded in breaking the BM. The invading cells developed actin-rich protrusions on their ventral side, which corresponded to the holes in the BM (Fig. 1 C and not depicted). These protrusions were from 1 to 7 µm long and ranged from 0.5 to 2 µm in diameter (on average 1.15 ± 0.88 µm; $n = 117$; stages 1 and 2). In the later stages of invasion, a large area of the cell protruded through the hole (stage 3). Although most cells were in stage 1 within 1 d after the incubation, they reached stage 2 between 3 and 5 d and stage 3 after 5 d (Fig. 1 D). After 7 d, the majority of cells had moved across the BM, as previously reported (Hotary et al., 2006). Because the protrusions developed in stages 1 and 2 appeared similar to invadopodia, we determined whether they contained the same molecular components (Fig. 2). Cortactin and MT1-MMP, the two best-described invadopodial markers (Nakahara et al., 1997; Bowden et al., 1999, 2006), were also localized in the cellular protrusions developed on the native BM; although cortactin (Fig. 2 A) was present all along, MT1-MMP was located primarily at the base of these protrusions (Fig. 2 B). An active form of c-src was also detected in these protrusions, as it has been reported for invadopodia (Fig. 2 C; Chen, 1989; Buccione et al., 2004; Weaver, 2006; Linder, 2007). These observations suggest the following sequence of events as invasive cancer cells penetrate into the underlying stroma: short protrusions (henceforth referred to as invadopodia) degrade the BM (stage 1) and then elongate into longer protrusions (mature invadopodia; stage 2) that then guide the cell body to deform through the hole and enter the stromal compartment (stage 3).

In vitro assays used to mimic the formation and elongation of invadopodia

To mimic stage 1 of invasion, we used a typical invadopodia assay, whereby cancer cells are cultured on a thin layer of fluorescently labeled gelatin (Artym et al., 2006, 2009). Within 5–6 h, MDA-MB-231 cells degraded the fluorescent ECM, producing dark spots in the fluorescent background. Invadopodia were defined as an accumulation of F-actin at the ventral surface of the cells that localized to the sites of matrix degradation (Fig. S1). The thickness of the gelatin layer covering the glass coverslip limited the length of the invadopodia. Thus, to mimic the second stage of invasion, we developed a new experimental technique: the chemoinvasion assay. All experiments were performed using two cell lines, MDA-MB-231 and HCT116. Cells were plated

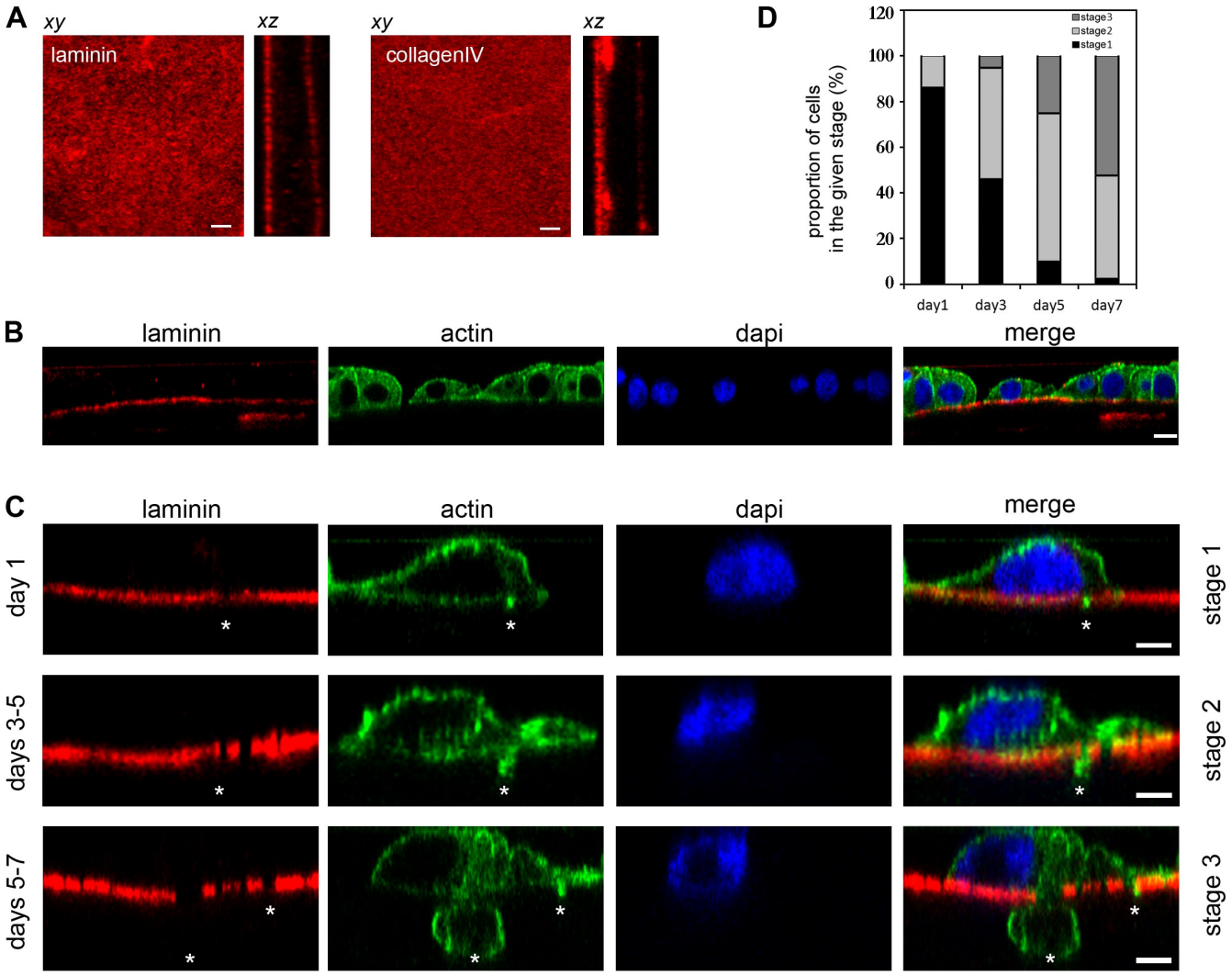

Figure 1. **Stages of BM breakage by invasive cancer cells.** (A) Mesothelial BM. (left panels) x–y images showing the top of the BM immunostained for laminin (left) or collagen IV (right). (right panels) x–z sections of the corresponding x–y projection revealing the two BM layers present in the rat peritoneum. (B and C) Cells cultured atop of peritoneal BM stained with phalloidin–Alexa Fluor 488 (green) and DAPI (blue). BM was detected by laminin staining (red). Merged images are shown in the right column. HT29 (B) and HCT116 (C) cells are shown. (top) Stage 1, early stage of invasion characterized by degradation of the BM and formation of short invasive protrusions (invadopodia). (middle) Stage 2, intermediate stage of invasion and formation of long invasive protrusions (mature invadopodia). (bottom) Stage 3, late stage of invasion and infiltration of the cell on the other side of the membrane. Asterisks indicate sites of degradation and localization of invasive protrusions. (D) Time requirement for BM penetration by HCT116 cells. Black bars show the percentage of cells in stage 1. Light gray bars show the percentage of cells in stage 2. Dark gray bars show the percentage of cells in stage 3. Bars: (A and C) 5 µm; (B) 10 µm.

on filters containing 1-µm-diameter pores, covered by a thin layer of fluorescently labeled Matrigel to mimic the BM, and chemoattracted using serum and hepatocyte growth factor (HGF)–enriched medium. Only the first 2 µm of the pores were reliably covered and filled with Matrigel, but deeper parts were mostly open-spaced, as in all commercially coated filters (unpublished data). The pore size chosen corresponded to the mean diameter of invadopodia but was smaller than the cell nucleus. As a consequence, cells formed invadopodia without passing through the filter. In addition, the thickness of the filter (~11 µm) permitted the elongation of invadopodia inside the pores (Fig. 3 A). In this assay, within 15 h, the cells remodeled the matrix and formed actin-rich protrusions that were an average of 6.9 ± 0.5 µm long, reaching a maximum length of ~12 µm (Fig. 3 B). To verify that the formation of these invasive protrusions was dependent on matrix degradation, MDA-MB-231 cells were treated with a general MMP inhibitor, GM6001. After GM6001 treatment, the number of cells able to degrade the gelatin matrix was reduced by 67 ± 1%. Similarly, the number of cells forming invasive protrusions in the chemoinvasion assay was decreased by 59 ± 2% compared with control cells (Fig. 3 C), as previously shown (Ayala et al., 2008). In addition, the noninvasive HT29 cancer cells were neither able to degrade the gelatin matrix nor able to form mature invadopodia in the chemoinvasion assay (unpublished data). Therefore, the activity of MMPs was required in both assays for the formation of invadopodia.

Protein composition of invadopodia

Using the gelatin degradation assay, we first examined whether molecular markers that discriminate between bundled and

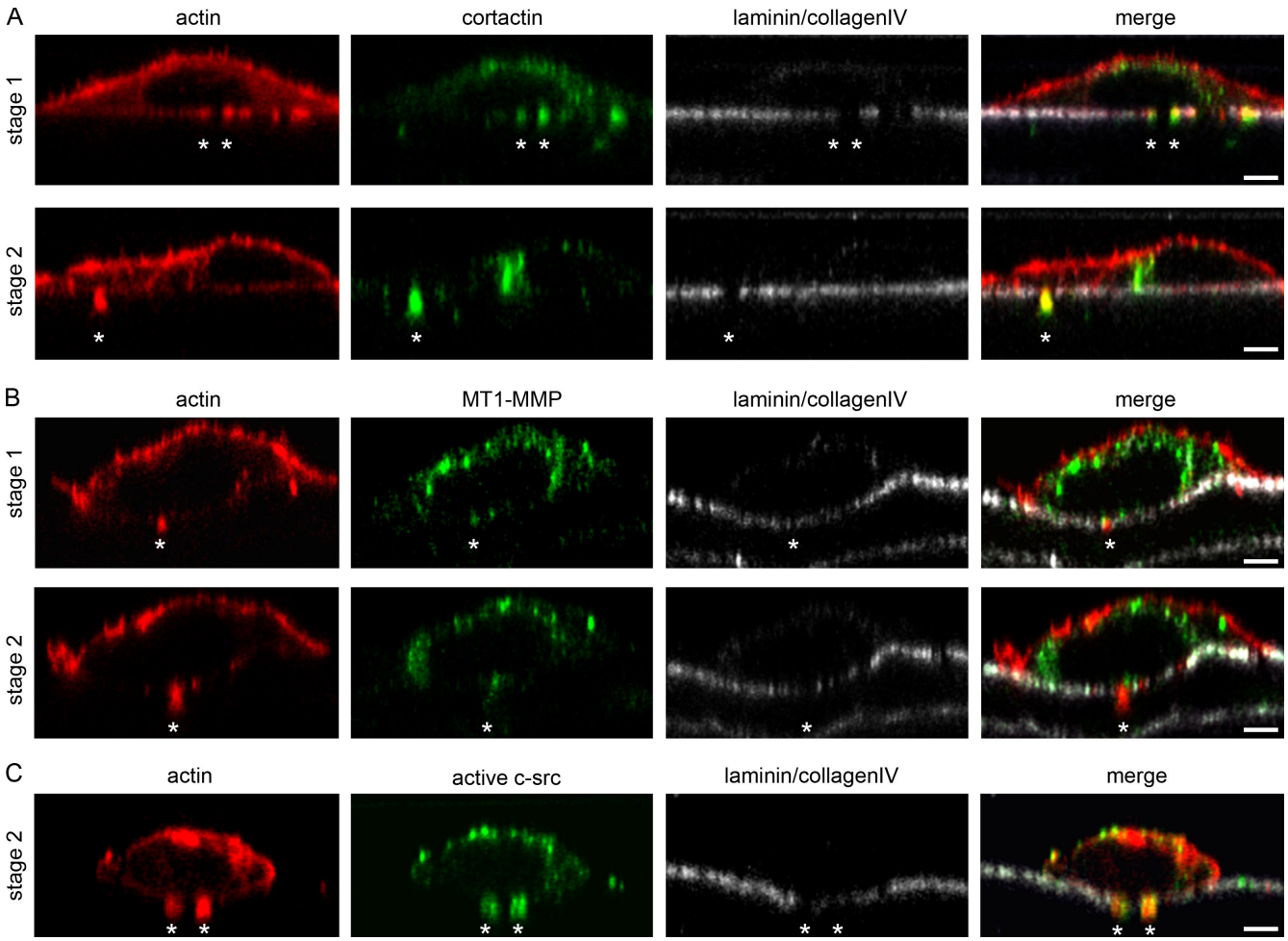

Figure 2. **Invasive cancer cells form invadopodia on the native BM.** (A–C) Localization of invadopodia markers in invasive protrusions: cortactin (A), MT1-MMP (B), and c-src (C). From left to right, columns show actin revealed by phalloidin-Cy3 (red), invadopodia markers as indicated (green), BM detected by immunostaining for laminin and collagen IV (gray), and merged images. Asterisks indicate invasive protrusions. Bars, 5 µm.

dendritic actin networks are present in invadopodia (stage 1). Besides confirming the previous findings that cortactin (Bowden et al., 1999, 2006; Clark et al., 2007) and Arp2/3 (Bowden et al., 1999; Yamaguchi et al., 2005; Clark et al., 2007) are enriched in invadopodia, we found that two other lamellipodial markers, capping protein and α-actinin, were also localized in invadopodia (Fig. 4 and Fig. S1). mDia2 and VASP, two common markers of lamellipodia and filopodia, were also accumulated at the degradation sites (Fig. 4 and not depicted), as recently reported (Philippar et al., 2008; Lizárraga et al., 2009). Finally, we observed that the specific markers of filopodia, fascin, T-fimbrin, and myosinX, were also concentrated in invadopodia (Fig. 4 B and Fig. S1). Together, this molecular marker analysis suggests that invadopodia represent a hybrid structure displaying enrichment of lamellipodia- and filopodia-associated proteins.

Formation of invadopodia requires filopodial and lamellipodial molecular machinery

Several of the lamellipodial and filopodial proteins such as Arp2/3 (Yamaguchi et al., 2005), cortactin (Artym et al., 2006; Clark et al., 2007), Mena/VASP (Philippar et al., 2008), and mDia2 (Lizárraga et al., 2009) are involved in matrix degradation and invadopodia activity. To investigate whether other actin-related proteins present in invadopodia have a specific role in invadopodia formation, we compared the capacities of cells treated with specific siRNAs (Fig. 5 A) to degrade the gelatin matrix using two parameters: (1) the proportion of cells able to degrade the matrix and (2) the extent of degradation represented as a degradation index. We observed that ∼20% of cells treated with control siRNA degraded the matrix, similarly to mock-treated cells (unpublished data). Depletion of fascin or myosinX resulted in a 40–50% reduction in the number of cells able to degrade the matrix, whereas knockdown of p34, a subunit of the Arp2/3 complex, reduced this number ∼30% (Fig. 5 B). To quantify the extent of matrix degradation, we measured the total degraded area. The degradation index of Arp2/3- and myosinX-depleted cells was decreased by 60% and 70%, respectively, similar to the level observed for mDia2 knockdown (Lizárraga et al., 2009). Fascin-depleted cells showed an intermediate phenotype, with a 45% reduction of the degradation index (Fig. 5 C). Depletion of T-fimbrin did not have any effect on invadopodia formation and function (unpublished data). Simultaneous depletion of T-fimbrin and fascin had the same effect

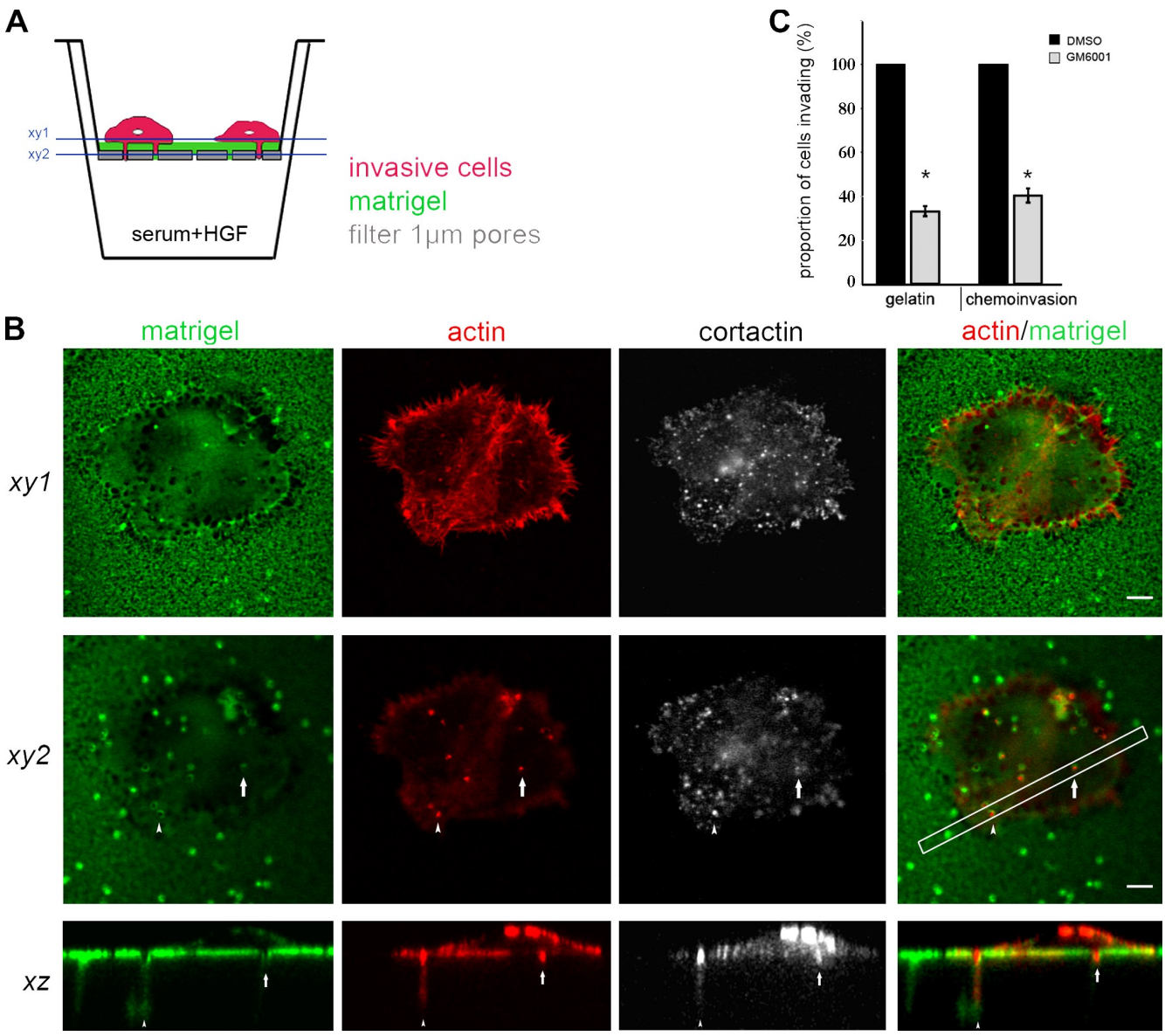

Figure 3. **Invadopodia elongation and chemoinvasion assay.** (A) Schematic diagram of the chemoinvasion assay. Blue lines correspond to the x–y planes shown in B. (B) HCT116 cells in the chemoinvasion assay. Fluorescent Matrigel, actin stained with phalloidin-Cy3, cortactin, and a merged image of actin and Matrigel are shown. (top) x–y projections presenting the cell on the top of the filter. (middle) x–y projections presenting the cell below the focal plane of the filter. Arrows and arrowheads indicate a short and long protrusion, respectively. On the merged picture, the white rectangular corresponds to the longitudinal cut shown in the bottom panels. (bottom) x–z projections showing longitudinal cut through the cell at the level of the protrusions. (C) Effect of the metalloprotease inhibitor GM6001 on the formation of invadopodia. (left) Gelatin assay shows the percentage of cells that degraded the gelatin. (right) Chemoinvasion assay shows the percentage of cells that formed mature invadopodia. The results were normalized to the cells treated with DMSO. Light gray bars correspond to the cells treated with 10 µM GM6001. Dark gray bars correspond to control DMSO-treated cells. Error bars indicate SEM. *, $P < 0.001$; paired *t* test. Bars, 5 µm.

as the depletion of fascin alone (unpublished data), suggesting that fascin is the major actin bundler in invadopodia. Thus, invadopodia formation requires the same molecular machinery as filopodia and lamellipodia.

Finally, we wondered which actin structure (branched or bundled) is important for the stability of the invadopodial actin core. Thus, we analyzed the lifetime of remaining invadopodia (using mCherry-LifeAct as a tracking marker) upon depletion of the Arp2/3 complex as a branch-generating protein and fascin and myosinX as actin bundle–associated proteins (Fig. 5 D). In control cells, the lifetime of invadopodia varied from minutes to several hours. The majority of invadopodia persisted for periods ranging from 20 to 80 min, with 20% persisting for >2 h (i.e., long-lived invadopodia; Video 1). Depletion of fascin and, even more strikingly, depletion of the Arp2/3 complex inhibited the formation of long-lived invadopodia. Most of the invadopodia from Arp2/3-depleted cells had a lifetime of 20–40 min (Video 2), whereas invadopodia from fascin-depleted cells persisted for 40–60 min. In contrast, depletion of myosinX did not significantly affect the lifetime of invadopodia. Together, these results indicate that both branched and bundled actin structures have a role in the stabilization of invadopodia.

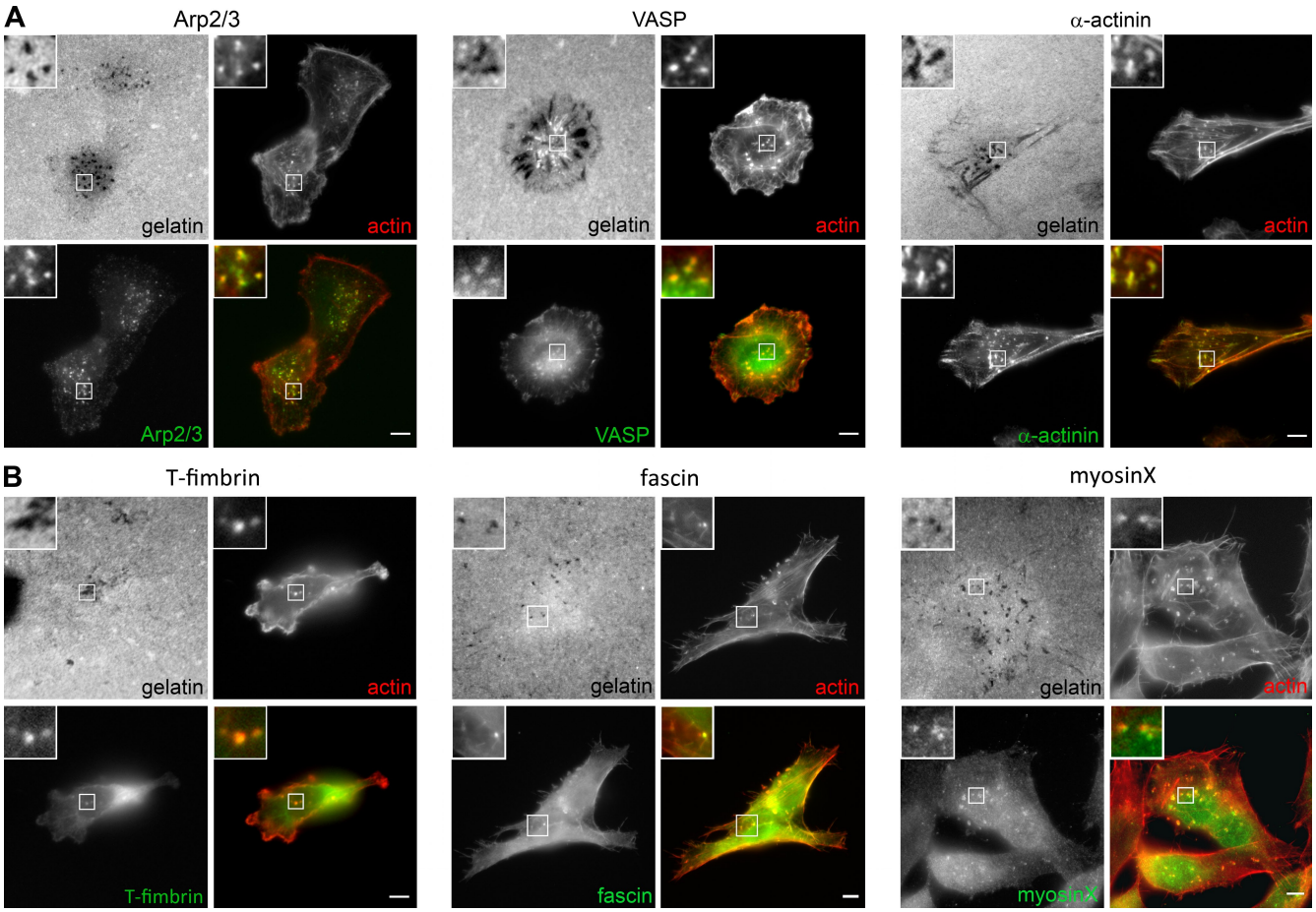

Figure 4. **Lamellipodial and filopodial markers are present in invadopodia.** (A and B) Immunofluorescence analysis in the gelatin degradation assay. (top left) Fluorescently labeled gelatin. (top right) Actin revealed by phalloidin-Cy3. (bottom left) ABP as indicated. (bottom right) Merged image of ABP (green) and actin. Insets show higher magnification images of the boxed regions. (A) ABPs associated with lamellipodia revealed by immunostaining (p34 subunit of Arp2/3 complex) or by expression of GFP fusion proteins (VASP and α-actinin) in MDA-MB-231 cells. (B) ABPs associated with filopodia visualized by expression of GFP fusion proteins (T-fimbrin in MDA-MB-231 cells; fascin and myosinX in MDA-MB-435 cells). Bars, 5 µm.

Protein distribution in mature invadopodia

We hypothesize that lamellipodia- and filopodia-associated molecules cooperate in the formation of invadopodia: the Arp2/3 complex and mDia2 could be required for the generation of actin filaments, which are further elongated by mDia2, VASP, and myosinX and ultimately bundled by fascin and T-fimbrin. This would permit invadopodia to protrude through the degraded BM to reach the stroma. The increase in the spatial resolution gained using the chemoinvasion assay made it possible to analyze the distribution of actin-associated molecules along mature invadopodia (stage 2) by immunostaining or expression of GFP-tagged proteins (Fig. 6 and Fig. S2). We verified that soluble GFP was not enriched in mature invadopodia, indicating that enrichment of the GFP-tagged proteins in such protrusions was not simply a result of diffusion (unpublished data). The length of mature invadopodia was determined by staining for actin. The protrusions were classified into two groups according to their length: short (<5 µm) and long protrusions (>5 µm). We first examined the distribution of lamellipodia markers. Cortactin was localized throughout the protrusions independently of their length. In HCT116 cells, Arp2/3 colocalized with actin all along the length of short protrusions (n = 25), whereas in the majority of long protrusions (75%; n = 26), it was limited to their base (Fig. 6 A and Fig. S3 B). In MDA-MB-231 cells, the Arp2/3 complex was localized along the shafts of the majority of mature invadopodia (90%; n = 34; Figs. S2 and S3 A). Although the extension of the actin branched network generated by the Arp2/3 complex remained variable and cell type dependent, the Arp2/3 complex was never enriched at the tip of the protrusions. We next analyzed the localization of α-actinin, VASP, and mDia2 as common markers of lamellipodia and filopodia (Fig. 6, A and B). α-Actinin and VASP were present along the shaft of mature invadopodia independently of their length. Because VASP can bind to actin barbed ends, its distribution could reveal fluctuations in the length of actin filaments within the protrusion. Although full-length mDia2 was mostly cytoplasmic, as reported previously (Alberts, 2001; Yang et al., 2007), careful analysis showed that it was localized all along the shafts of invadopodia (Fig. 6 B) and sometimes enriched at their tips. However, an active form of mDia2 (ΔGBD-mDia2) that exhibited relatively low cytoplasmic fluorescence localized at the tips of the majority of long mature invadopodia in MDA-MB-231 cells (Figs. S2 C and S3 A). In HCT116 cells, the distribution of ΔGBD-mDia2 was heterogeneous (Figs. S2 D and S3 B).

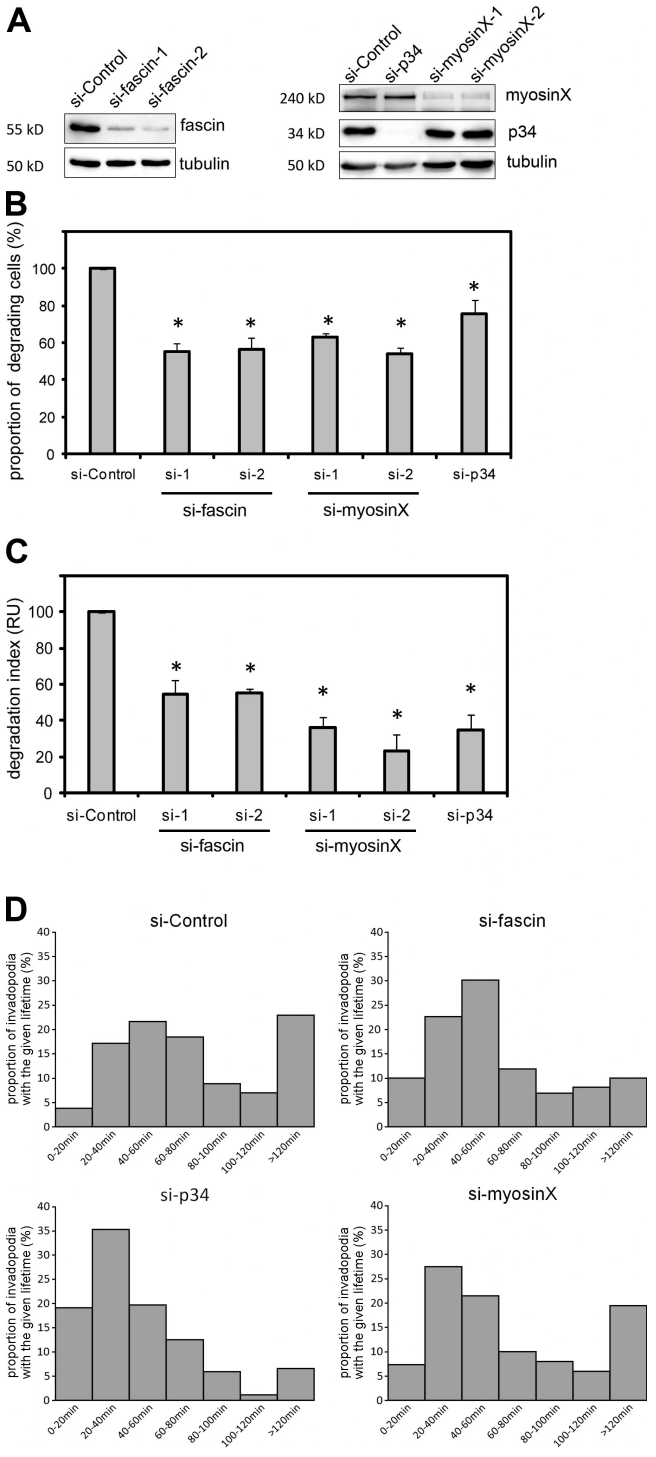

Figure 5. **The formation of invadopodia relies on lamellipodia and filopodial machineries.** (A) Immunoblot analysis after siRNA treatment. Scrambled siRNA served as a control for the nonspecific cell response (si-control). Tubulin served as a loading control. (B and C) Quantification of the gelatin degradation of MDA-MB-231 cells treated with the indicated siRNA and normalized to the cells treated with a scrambled siRNA (si-control). (B) Percentage of cells that degraded the gelatin. (C) Degradation index was calculated as described in Materials and methods. (B and C) Error bars indicate SEM. *, $P < 0.001$; Kruskal-Wallis analysis of variance, Holm-Sidak method. (D) Time-lapse analysis of invadopodia lifetime. Each graph shows the distribution of invadopodia lifetimes in each of the conditions as indicated. Statistical differences were observed between si-control and si-fascin and si-control and si-p34 but not between si-control and si-myosinX ($P < 0.001$; Kruskal-Wallis analysis of variance, Dunn's method).

Finally, we determined the spatial distribution of the filopodial components fascin, T-fimbrin, and myosinX. The actin-bundling proteins fascin and T-fimbrin were uniformly distributed along mature invadopodia (Fig. 6 B). MyosinX was concentrated at the tips of most invadopodia (55%; $n = 28$; Fig. 6 B; and Fig. S3, A and B). In conclusion, we observed that the spatial distribution of fascin, T-fimbrin, and myosinX and often mDia2 in mature invadopodia resembles that present in filopodia. The localization of lamellipodial markers suggests that the base or the whole shaft of mature invadopodia is embedded in a dendritic actin network.

Elongation of invadopodia requires both the molecular machinery of filopodia and lamellipodia

The roles of the two actin assembly machinery in invadopodia elongation were investigated by RNAi. We perturbed the filopodial machinery by depleting myosinX, mDia2, or the actin bundlers fascin and T-fimbrin, whereas the dendritic actin network was removed by depleting the Arp2/3 complex (Fig. 6 C and Fig. S3 C). Cells treated with a control siRNA almost had an equal distribution of short and long protrusions. Individual depletion of actin bundlers fascin or T-fimbrin decreased the number of long protrusions. Simultaneous depletion of the two bundlers had an additive effect, decreasing the number of long invadopodia even further, resulting in 20% of long invadopodia (Fig. 6 D and Fig. S3 D). These observations suggest a compensative effect between fascin and T-fimbrin in the chemoinvasion assay. Depletion of myosinX and mDia2 had an effect similar to the simultaneous depletion of the two actin-bundling factors, whereas silencing of the Arp2/3 complex had less of an impact, as indicated by the retention of 35% of the long protrusions. These results show that although the elongation of invadopodia requires both filopodia- and lamellipodia-associated proteins, it is more dependent on the bundled actin network. Finally, depletion of Arp2/3, fascin, and myosinX, the major proteins involved in the elongation of invadopodia, resulted in a reduction in the length of the protrusions in the native BM model to approximately the same extent as detected in the chemoinvasion assay (Fig. 6 E).

The ultrastructural organization of the cytoskeleton in mature invadopodia

Next, we used the chemoinvasion assay to study the ultrastructural organization of the cytoskeleton in mature invadopodia using transmission EM (Fig. 7 and Fig. S4). In the early stages of invasion, we observed several invadopodia entering one pore, resembling what was previously observed on the gelatin matrix (Chen, 1989; Bowden et al., 1999). However, in the later stages of invasion, only a single mature invadopodium could be observed per pore. The organization of the actin network was difficult to determine because of the restrictive sectioning angle required to cut through invadopodia. Nevertheless, a careful analysis of the micrographs revealed dotty staining on the sides and base of the protrusions that most likely represents short pieces or cross sections of randomly arranged filaments in a dendritic/diagonal actin network, as is typically

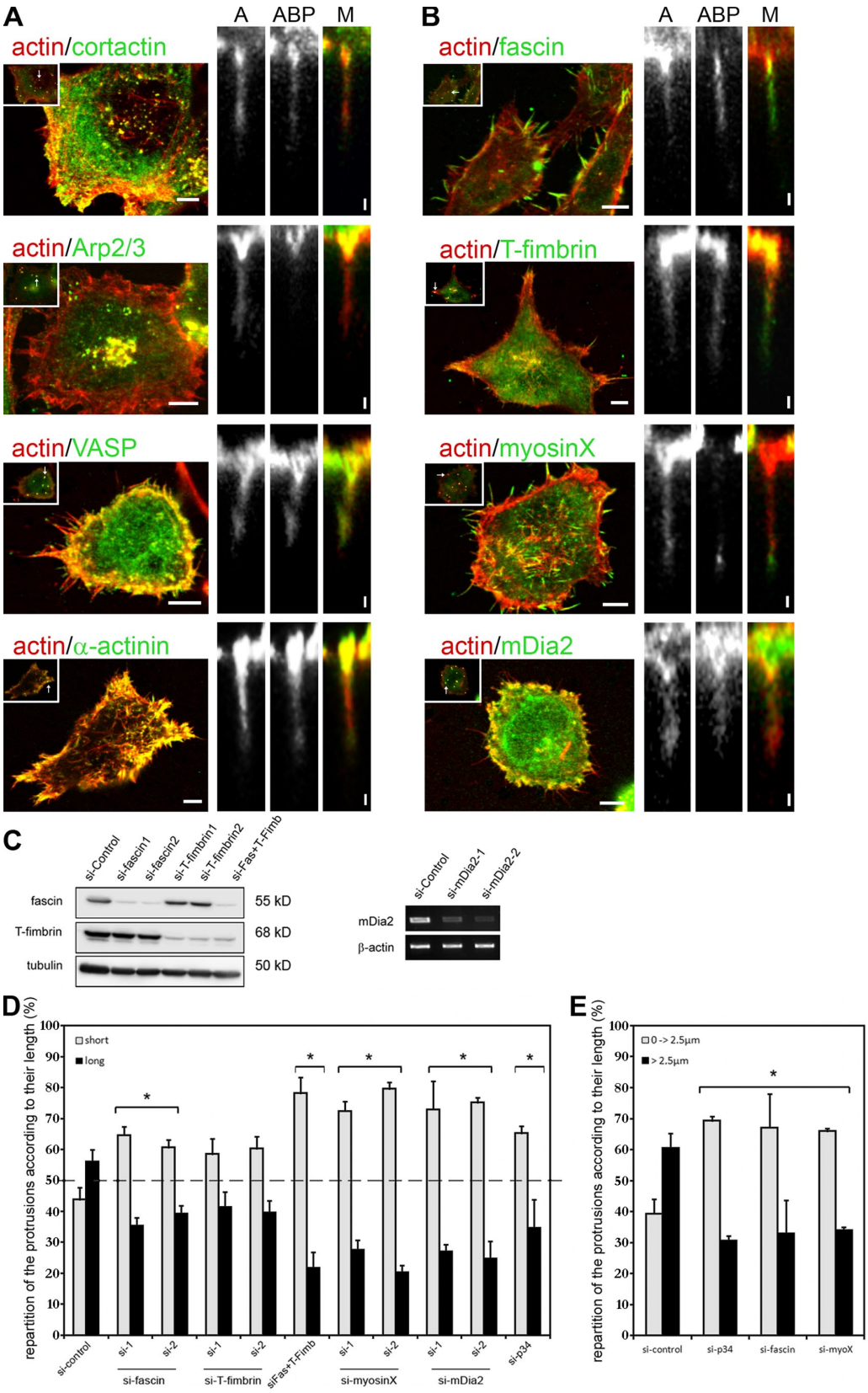

Figure 6. **The elongation of invadopodia relies on lamellipodial and filopodial machinery.** (A and B) Immunofluorescence analysis of HCT116 cells in the chemoinvasion assay: spatial distribution of lamellipodial and filopodial markers in mature invadopodia. (left) x–y projections of the cell at the focal plane of the filter. The image is merged, showing actin revealed by phalloidin-Cy3 and the specified ABPs (green). Insets show the x–y projections of the ventral surface of the cell at the focal planes below the filter. Arrows indicate invasive protrusions. (right) z projections of the indicated protrusion. A, actin (red); ABP, ABP as specified in the left panels (green); M, merge. (A) ABPs associated with lamellipodia revealed by immunostaining (cortactin and p34 subunit of Arp2/3 complex) or by expression of GFP fusion proteins (VASP and α-actinin). (B) ABPs associated with filopodia visualized by immunostaining (myosinX)

observed on thin sections of lamellipodia by EM (Maupin and Pollard, 1983). Moreover, a dense array of thin filaments resembling actin bundles was consistently visible at the very tip of the protrusions or at the sides of the invadopodia. Unfortunately, the individual filaments in these bundles were difficult to resolve because they were tightly packed. In addition to these putative actin filaments, in the core of the mature invadopodia, we observed filaments larger in diameter (10–15 nm) innervating two thirds of the length of the protrusion. Based on their diameter and overall appearance, we identified these structures as intermediate filaments. Unstained intermediate filaments have a diameter of 7–10 nm, but staining with tannic acid increases the electron density of all filaments, resulting, on average, in 16-nm-thick intermediate filaments. Because of their stability, these filaments were very well preserved even after preextraction of the cell (Fig. S4 E). Typically, one to two microtubules (filaments of average 22 nm in diameter) per section and per protrusion were observed embedded in the intermediate filament network. Finally, many vesicles/endosomes were observed inside the protrusions, illustrating the presence of active traffic in mature invadopodia.

Microtubules are required for the elongation but not for the formation of invadopodia

The unexpected presence of microtubules and intermediate filaments in mature invadopodia observed by EM raised the question of their role in invadopodia formation, maturation, and subsequent cell invasion. Using the gelatin degradation assay, we showed that microtubules were not present in invadopodia (Fig. 8 A). Next, using the chemoinvasion assay, we found that microtubules penetrated mostly into long invadopodia (Fig. 8 B and Fig. S5 A). To investigate whether microtubules in invadopodia are dynamic, we examined the subcellular distribution of tyrosinated tubulin (tyr-tubulin), which marks a relatively dynamic subclass of microtubules (Fig. 8 B and Fig. S5 A; Kreis, 1987). We found that dynamic microtubules were restricted to the base of invadopodia, demonstrating that microtubules in invadopodia shafts are stable.

Microtubule depolymerization by nocodazole treatment (Fig. 8 C) did not affect the formation of invadopodia (Fig. 8 D) but led to a decreased number of long invadopodia compared with control cells (Fig. 8 E and Fig. S5 B). Besides confirming the previous finding that microtubules are not required for invadopodia formation (Kikuchi and Takahashi, 2008), these results demonstrate that microtubules are required for invadopodia elongation.

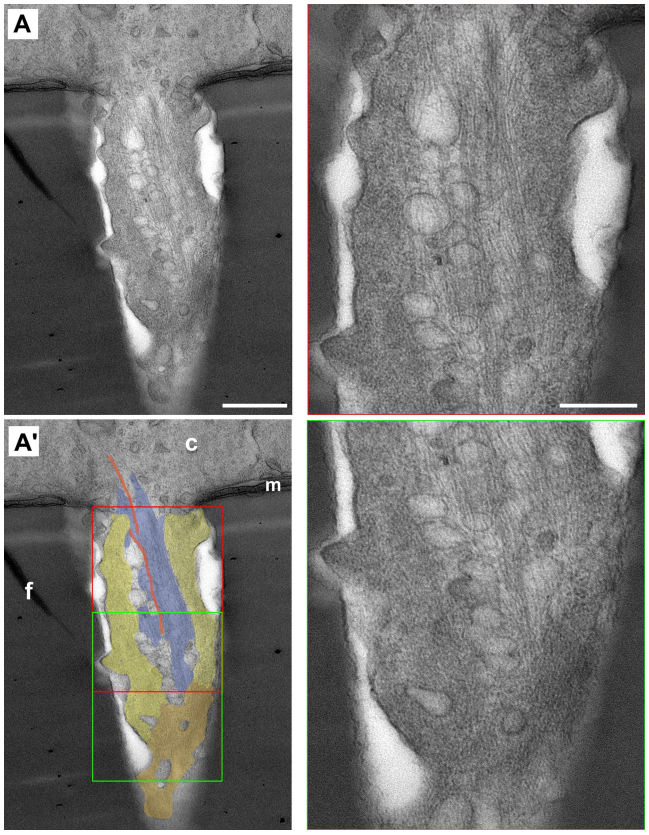

Figure 7. **Electron micrographs of invadopodia.** (A) Mature invadopodia in MDA-MB-231. (A′) The same invadopodia in which the cytoskeleton networks were color coded: microtubules in orange, intermediate filaments in blue, and actin in light/dark yellow. The majority of the actin filaments are randomly arranged so that only short pieces or cross sections are seen in a thin section (light yellow). Bifurcation of actin bundle at the tip of the invadopodia (dark yellow) is shown. Images on the right are a higher magnification of the corresponding boxed regions in A′. Red indicates the base/central part of mature invadopodia; green indicates the central/tip part of mature invadopodia. c, cell; f, filter; m, Matrigel. Bars: (A and A′ [left]) 0.5 µm; (A′, right) 0.25 µm.

Vimentin intermediate filaments are required for the elongation but not for the formation of invadopodia

First, using the gelatin degradation assay, we showed that neither vimentin nor cytokeratin intermediate filaments were present in invadopodia (Fig. 9 A). Second, using the chemoinvasion

or by expression of GFP fusion proteins (fascin, T-fimbrin, and mDia2). For the visualization of fascin, the nonphosphorylatable mutant (S39A) was used. (C and D) Effect of the depletion of lamellipodial and filopodial machinery on the elongation of invadopodia in MDA-MB-231 cells in the chemoinvasion assay. (C, left) Immunoblot analysis after siRNA treatment. Scrambled siRNA served as a control for the nonspecific cell response (si-control). Tubulin served as a loading control. (right) mRNA expression levels of mDia2 in the cells transfected with two independent siRNA against mDia2 and control siRNA. β-Actin mRNA levels were used as a loading control. (D) Repartition of the protrusions according to their length in cells transfected with siRNA as indicated. Light gray bars show short protrusions (<5 µm). Black bars show long protrusions (>5 µm). The dashed line (50%) is shown to compare the distribution of protrusion lengths between control and siRNA-treated cells. *, $P < 0.001$; Kruskal-Wallis analysis of variance, Holm-Sidak method. (E) Effect of the depletion of lamellipodial and filopodial machinery on the elongation of invadopodia in HCT116 cells in the native BM model. Repartition of the protrusions according to their length transfected with siRNAs is shown. Light gray bars show short protrusions (<2.5 µm). Black bars show long protrusions (>2.5 µm). *, $P < 0.001$; Kruskal-Wallis analysis of variance, Dunn's method. (D and E) Error bars indicate SEM. Fas, fascin; myoX, myosinX; T-Fimb, T-fimbrin. Bars: (A and B, left) 5 µm; (A and B, right) 1 µm.

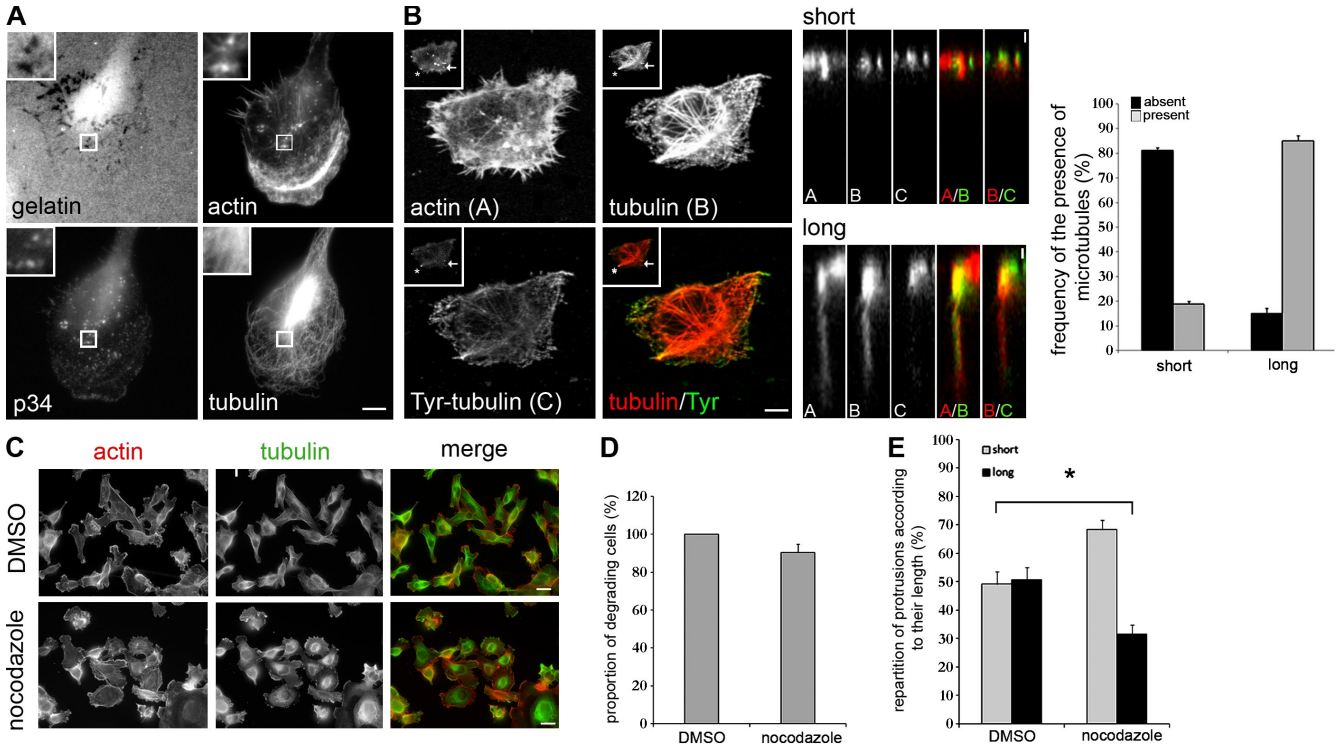

Figure 8. **Localization and role of microtubules during invadopodia formation and elongation.** (A) Gelatin degradation assay and localization of microtubules in invadopodia of MDA-MB-231 cells. (top left) Fluorescently labeled gelatin. (top right) Actin (phalloidin-Cy3). (bottom left) The Arp2/3 complex (immunostaining for the p34 subunit). (bottom right) Microtubules (immunostaining for tubulin). Insets show higher magnification images of the boxed regions. (B) Chemoinvasion assay and localization of microtubules in mature invadopodia of HCT116 cells. (left) x–y projections of the cell above the focal plane of the filter. (top left) Actin (phalloidin-Cy3). (top right) Microtubules (immunostaining for tubulin). (bottom left) Tyr-tubulin. (bottom right) Merged image of tubulin and tyr-tubulin (Tyr). Insets show x–y projections of the cell below the focal plane of the filter. Arrows and asterisks indicate protrusions shorter and longer than 5 µm, respectively. (middle) z projections of the indicated protrusions. A, actin; B, tubulin; C, tyr-tubulin; A/B and B/C, merged images as indicated. (right) Presence or absence of microtubules in invasive protrusions according to their length. (C) Immunofluorescence analysis after disruption of the microtubule network by nocodazole in MDA-MB-231 cells. Cells were treated with 5 µM DMSO or 5 µM nocodazole for 5 h. Actin revealed by phalloidin-Cy3, microtubules revealed by immunostaining for tubulin, and merge pictures are shown. (D) Quantification of the gelatin degradation of MDA-MB-231 cells treated with the specified reagent and normalized to their respective controls. Cells treated with 5 µM nocodazole were compared with DMSO-treated cells. The results of DMSO- versus nocodazole-treated cells were not statistically different ($P = 0.1$ and $P = 1$; Mann-Whitney rank sum test). (E) Repartition of the protrusions according to their length in MDA-MB-231 cells treated with 2 µM DMSO or nocodazole. Light gray bars show short protrusions (<5 µm). Black bars show long protrusions (>5 µm). *, $P < 0.001$; Mann-Whitney rank sum test. (B, D, and E) Error bars indicate SEM. Bars: (A and B [left]) 5 µm; (B, middle) 1 µm; (C) 20 µm.

assay, we found that cytokeratins were present in most of the mature invadopodia independently of their length (Fig. 9 B and Fig. S5 C). However, vimentin filaments penetrated mostly into long invadopodia. To investigate whether vimentin filaments were required for invadopodia elongation, we measured the length of invadopodia in MDA-MB-231 cells after depletion of vimentin using siRNA (Fig. 9, C and D) or disruption of vimentin filaments using a dominant-negative vimentin probe (Fig. 9, E and F; Kural et al., 2007). On whole cell population, knockdown efficiency was 50% measured by Western blot (Fig. 9 C). Because immunofluorescence revealed strong cell to cell differences in vimentin knockdown, we studied invadopodia elongation using cells that were >80% depleted of vimentin. Both approaches demonstrated that vimentin filaments are required for the elongation of invadopodia. Finally, we asked whether keratin filaments have an overlapping function with vimentin in invadopodia elongation. We found that vimentin depletion from a keratin-free cell line, MDA-MB-435, did not have an additional effect on invadopodia length (Fig. S5, D–F). In conclusion, elongation of invadopodia is dependent on an intact vimentin network.

Discussion

Carcinomas develop on the epithelial side of the BM and are considered to be benign as long as tumor cells stay encapsulated by the BM. Dissolution of the BM by invading cancer cells removes the physical barrier for further cancer expansion; thus, it is a critical step in the formation of metastasis. However, invasive cancer cells do not entirely digest the BM, but rather make small perforations. Growing evidence suggests that these perforations are the results of invadopodial activity (Buccione et al., 2004; Bowden et al., 2006; Linder, 2007; Weaver, 2008). Using a native BM, we provide evidence that after degrading the BM, invadopodia elongate to allow the penetration of cancer cells into the stroma (Fig. 10 A).

Formation of invadopodia

In this study, we show that the formation of invadopodia is dependent on the actin cytoskeleton, whereas microtubules and vimentin intermediate filaments are dispensable. We propose that both dendritic and bundled organizations of actin filaments

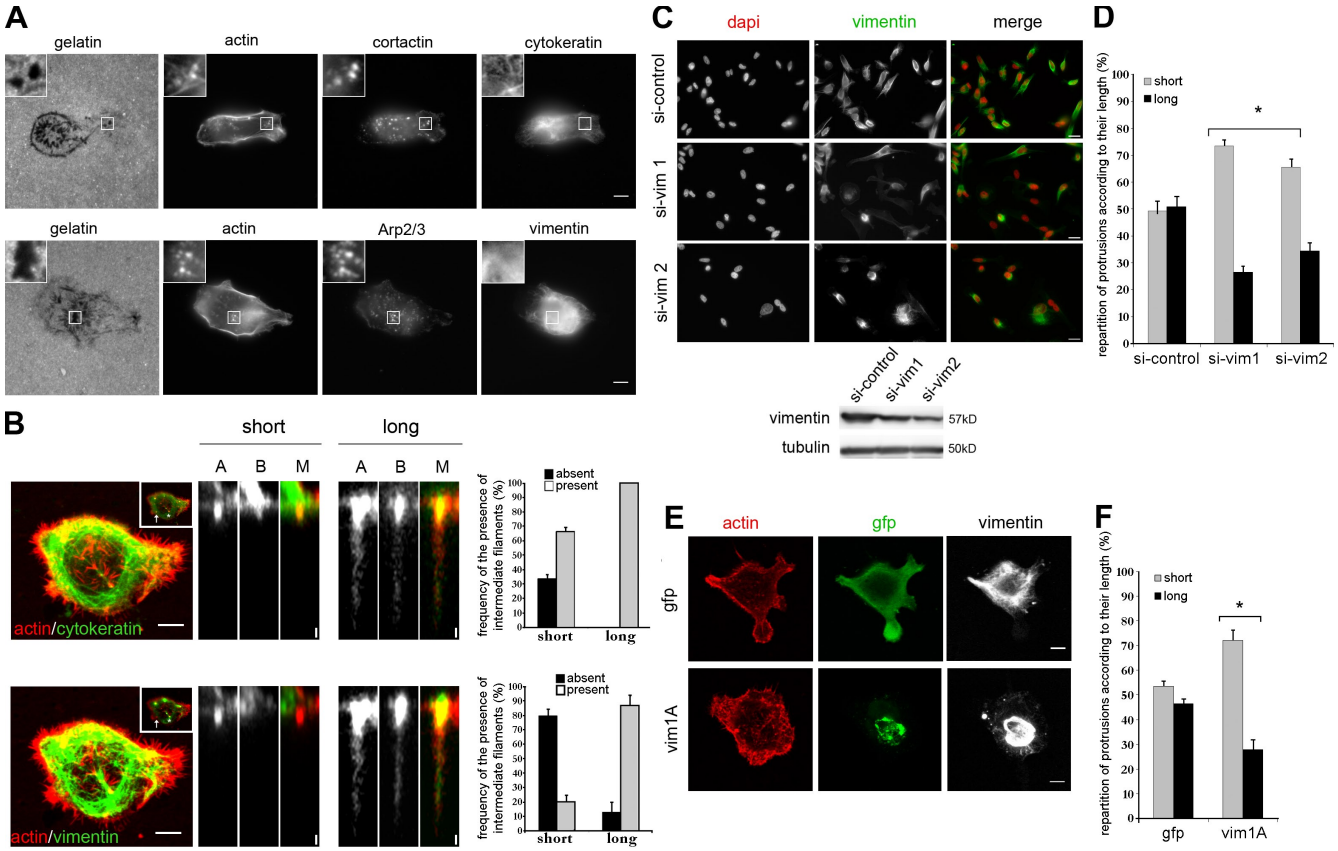

Figure 9. **Localization and role of intermediate filaments during invadopodia formation and elongation.** (A) Gelatin degradation assay using MDA-MB-231 cells. (top) Localization of cytokeratins. From left to right, fluorescently labeled gelatin, actin (phalloidin-Cy3), cortactin, and cytokeratin filaments are shown. (bottom) Localization of vimentin. From left to right, fluorescently labeled gelatin, actin (phalloidin-Cy3), the Arp2/3 complex, and vimentin filaments are shown. Insets show higher magnification images of the boxed regions. (B) Chemoinvasion assay and localization of intermediate filaments in mature invadopodia in HCT116 cells. (top) Cytokeratin filaments. (bottom) Vimentin filaments. (left) x–y projections of the cell above the focal plane of the filter. Merged images of actin and intermediate filaments (green) are shown. Insets show x–y projections of the cell below the focal plane of the filter. Arrows and asterisks indicate protrusions shorter and longer than 5 µm, respectively. (middle) z projections of the indicated protrusions. A, actin (red); B, intermediate filaments (green); M, merged image. (right) Presence or absence of intermediate filaments in invasive protrusions according to their length. (C, top) Immunofluorescence analysis after depletion of vimentin filaments by siRNA in MDA-MB-231 cells. DAPI (left), vimentin (middle), and a merged image (right) are shown. si-control indicates cells treated with a scrambled siRNA; si-vim1 and si-vim2 indicate cells treated with siRNAs against vimentin. (bottom) Immunoblot analysis after siRNA treatment. Scrambled siRNA served as a control for the nonspecific cell response (si-control). Tubulin served as a loading control. (D) Repartition of the protrusions according to their length in MDA-MB-231 cells treated with the indicated siRNA. Light gray bars show short protrusions (<5 µm). Black bars show long protrusions (>5 µm). *, $P < 0.001$; Kruskal-Wallis analysis of variance, Holm-Sidak method. (E) Immunofluorescence analysis of MDA-MB-231 cells transfected with pEGFP (gfp) or pEGFP-vim1A (vim1A) plasmids. Actin revealed by phalloidin-Cy3 (left), GFP (middle), and vimentin filaments revealed by immunostaining for vimentin (right) are shown. (F) Repartition of the protrusions according to their length in MDA-MB-231 cells transfected with pEGFP or pEGFP-vim1A. Light gray bars show short protrusions (<5 µm). Black bars show long protrusions (>5 µm). *, $P < 0.001$; Kruskal-Wallis analysis of variance, Dunn's method. (B, D, and F) Error bars indicate SEM. Bars: (A, B [left], and E) 5 µm; (B, middle) 1 µm; (C) 10 µm.

are required for the formation and activity of invadopodia. By analogy with lamellipodia and filopodia, the role of mDia2 in the generation of invadopodia could be to nucleate actin filaments in the vicinity of the plasma membrane, providing a starting material for Arp2/3-dependent nucleation of actin branches (Yang et al., 2007). As previously proposed, cortactin could recruit the Arp2/3 complex and its activator N-WASp to form an actin core in nascent invadopodia, which subsequently could act to stabilize the dendritic network of actin (Clark et al., 2007; Oser et al., 2009). Proteins specifically associated with actin bundles such as fascin and myosinX are also required for invadopodia formation. Although T-fimbrin is detected in invadopodia, its depletion does not appear to affect invadopodia number and the degree of matrix degradation (unpublished data). This suggests that T-fimbrin may not be primarily responsible for the initiation of actin bundles; the breakage of a highly cross-linked matrix (such as gelatin) may require stiffer bundles that could only be made by fascin. The depletion of the Arp2/3 complex and fascin decreased the lifetimes of invadopodia, indicating that both branched and bundled actin networks are necessary for the stability of the actin core. On the contrary, the depletion of myosinX did not affect invadopodia lifetime. Because lack of myosinX impairs matrix degradation, it probably functions as a molecular motor transporting molecules such as VASP (Tokuo and Ikebe, 2004) and possibly MMPs to invadopodia rather than as a glue clustering barbed ends as in filopodia (Bohil et al., 2006).

Elongation of invadopodia

Next, the growth of invadopodia and thereby their extension deeper into the substratum would require insertion of new

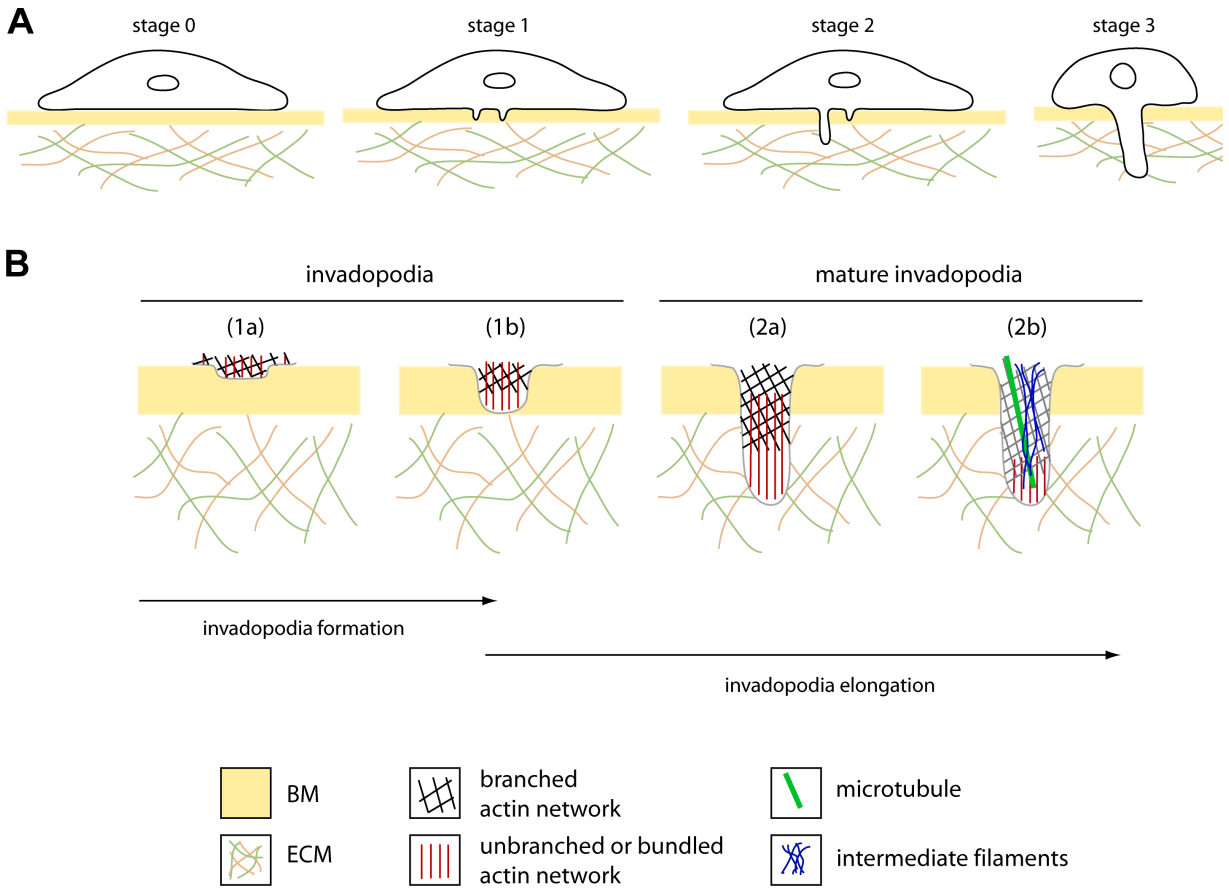

Figure 10. **Model for invadopodia formation and maturation.** (A) Stages of BM breaching by invasive cancer cells. Noninvasive tumor cells do not degrade the BM (stage 0). Once cancer cells become invasive, invadopodia form and degrade the BM (stage 1). Further, invadopodia elongate (stage 2) and lead the cell to infiltrate into the stromal compartment (stage 3). (B) Cytoskeleton organization in invasive protrusions. Formation of invadopodia requires the assembly of dendritic and bundled actin networks (1a). Elongation of invadopodia is achieved by growth of actin bundles, which is sustained by the dendritic actin network (1b and 2a). Microtubules and intermediate filaments penetrate mature invadopodia while actin bundles are replaced by the expansion of the dendritic actin network (2b).

membrane material into the plasma membrane, continuous delivery of MMPs, and an extension of the actin core structure. Lengthening of the actin structure could proceed by two divergent mechanisms. First, continued growth of the dendritic network could push the membrane and extend through the whole structure, resembling a lamellipodial protrusion. An alternative possibility is that actin bundles extend from the dendritic network to push at the membrane, a process resembling the formation of filopodia. In both scenarios, the elongation of the actin filaments is probably driven by mDia2 and VASP family members. The ultrastructural analysis of actin filament organization in mature invadopodia does not allow us to discriminate between these two possibilities, even though we attempted to preserve the actin filaments by lowering the concentration of OsO_4 and adding tannic acid to the fixation solution (Maupin and Pollard, 1983). However, the spatial and temporal distribution of major lamellipodia- and filopodia-related proteins suggests that mature invadopodia have a structure reminiscent of the roots of filopodia. In the latter structures, actin bundles are embedded in a dendritic actin network, as suggested by the finding that the actin-bundling proteins fascin and T-fimbrin are present along the shaft of mature invadopodia. Similar to filopodia, an active form of mDia2 and myosinX were detected at the tips of mature invadopodia, and the Arp2/3 complex was enriched at the base of mature invadopodia. In agreement with the latter observation, N-WASp activity and thus the activity of its downstream effector, the Arp2/3 complex, has been shown to be restricted at the base of the invadopodia (Lorenz et al., 2004). This eliminates the hypothesis of a comet tail–like architecture, in which a branched actin network is enriched at the tip of invadopodia (Baldassarre et al., 2006).

The primary role of invadopodia elongation is likely to be the focused degradation of the BM and underlying stroma. We suggest that the deep penetration capacity required for this process could be conferred by the bundling of actin filaments coupled with the focal delivery of proteases. Indeed, we showed in this study that bundling proteins fascin and T-fimbrin were necessary for invadopodia elongation. Similarly to its role in filopodia, myosinX could work as a molecular motor transporting molecules such as VASP (Tokuo and Ikebe, 2004) and possibly MMPs to the tip of invadopodia. Finally, the requirement of the lamellipodia-related proteins for invadopodia elongation suggests that the dendritic actin network could have a role in stabilizing growing actin bundles.

In addition to actin, microtubules were required for the elongation of invadopodia beyond the critical length of 5 µm

(Kikuchi and Takahashi, 2008; this study). Given their role in intracellular trafficking, it is possible that microtubules provide tracks for the delivery of specific proteins (such as MMPs) necessary for the elongation of invadopodia. The presence of microtubules and vesicles in mature invadopodia, as observed by EM, further supports this hypothesis.

Vimentin filaments have been shown to be present in podosomes of macrophages (Correia et al., 1999). However, we did not detect any class of intermediate filaments in invadopodia (stage 1), pointing out the structural differences between these two organelles. Interestingly, keratin and vimentin were present in mature invadopodia (stage 2), and we showed that an intact vimentin network was required for invadopodia elongation (Fig. 6, D and E; and Fig. S5 F). It is well established that intermediate filaments are involved in regulating cell shape and tissue homeostasis. Vimentin expression and a switch in keratin expression are always associated with the epithelial-mesenchymal transition and loss of cell–cell adhesions that take place during cancer invasion (Yilmaz and Christofori, 2009; Mendez et al., 2010). Moreover, vimentin is required for the motility and invasion of prostate cancer cells (Zhao et al., 2008). Thus, it is possible that intermediate filaments have a role in cell invasion by mechanically stabilizing mature invadopodia.

Model for invadopodia formation and maturation

In conclusion, we propose a model for cytoskeletal organization in invasive protrusions (Fig. 10 B). Dendritic and bundled actin networks are first assembled at the ventral surface of the cell providing a core for invadopodia formation (stage 1a). The actin core grows by elongation of actin bundles achieved by the filopodial machinery (stage 1b), further supported by dendritic network generated by the lamellipodia machinery (stage 2a). If the actin dendritic network advances as fast as the actin bundles elongate, the structure of the elongated invadopodium appears as a microspike (or roots of filopodia). Elongation of invadopodia beyond 5 µm is permitted by the infiltration of microtubules (stage 2b). Intermediate filaments are entering in mature invadopodia (2b) and have a role only in later stages of invasion (stage 3).

Materials and methods

Cell culture

MDA-MB-231, MDA-MB-435, and HCT116 cells were obtained from American Type Culture Collection and cultured in DME supplemented with 10% FCS (Invitrogen).

Plasmids, antibodies, and drugs

pEGFP–T-fimbrin, –α-actinin, -myosinX, and -VASP were provided, respectively, by J. Bartles (Northwestern University Medical School, Chicago, IL), C. Otey (University of North Carolina, Chapel Hill, NC), R. Cheney (University of North California), and F. Gertler (Massachusetts Institute of Technology, Cambridge, MA). pEGFP-mDia2 and –ΔGBD-mDia2 were a gift from A.S. Alberts (Van Andel Research Institute, Grand Rapids, MI). pcDNA3.1 MT1-MMP–HA was obtained from P. Chavrier (Institut Curie, Paris, France). pBabe c-src Y527F (active form of the chicken protein) was obtained from B. Elliott (Queen's University, Kingston, Ontario, Canada) as previously described (Hung and Elliott, 2001).

Monoclonal antifascin was purchased from Dako (clone 55K-2). Polyclonal anti-p34 and anti–chicken c-src and monoclonal anticortactin (clone 4F11) were purchased from Millipore. Polyclonal anti–T-fimbrin was obtained by M. Arpin (Institut Curie) as described in Arpin et al. (1994). Monoclonal anti–α-tubulin (clone DM 1A) and antivimentin (clone V9) and polyclonal anticytokeratin (wide spectrum screening) and antilaminin were purchased from Sigma-Aldrich. Polyclonal anti–mouse collagen IV was purchased from Millipore. Polyclonal anti-myosinX was a gift from R. Cheney. Polyclonal anti–tyr-tubulin was obtained from T. Kries (University of Geneva, Geneva, Switzerland) as described in Kreis (1987). Rhodamine-labeled phalloidin and all secondary antibodies were purchased from Invitrogen. The metalloproteinase inhibitor GM6001 was purchased from EMD and used at a final concentration of 10 µM. Nocodazole was purchased from Sigma-Aldrich. To disrupt microtubules, cells were treated with 5 µM nocodazole for 5 h in gelatin degradation assay or with 2 µM nocodazole for 15 h in chemoinvasion assay.

siRNA and plasmid transfections

For stable cells pools, MDA-MB-231 and MDA-MB-435 cells were transfected with Lipofectamine LTX reagent (Invitrogen), and HCT116 cells were treated with Nucleofector (Lonza) according to the manufacturers' protocols. The cells were selected with G418 at 0.8 mg/ml for MDA-MB-231 cells and at 0.5 mg/ml for HCT116. After 3 wk of selection, the positive cells were enriched by FACS for GFP-expressing cells. MDA-MB-231 cells stably expressing ABP (LifeAct) tagged with Cherry (mCherry-LifeAct) were obtained from P. Chavrier (Lizárraga et al., 2009).

RNAi experiments were performed 72 h after siRNA transfection with Lipofectamine RNAimax reagent (Invitrogen). The siRNAs used in this study were purchased from Thermo Fisher Scientific (see Table I for the list and the concentration used for each siRNA). For vimentin depletion, cells were transfected two times with 20 nM siRNA.

Reverse transcription–PCR

Total RNA was obtained using the RNeasy Mini kit from QIAGEN. cDNA synthesis was performed using SuperScript III reverse transcription enzyme (Invitrogen). PCR reactions were performed using Taq red DNA Polymerase (Invitrogen) with primers for human DRF3 mRNA (5′-CGTACCACTGGCATCGTGAT-3′ and 5′-GTGTTGCGTACAGGTCTTTG-3′) and primers for β-actin mRNA as a control for loading (5′-AGCAGAGCGAGAAAGACTCG-3′ and 5′-GGACTGAGACTCTGCCGAAC-3′).

Immunoblotting

Cells were washed with PBS and immediately lysed in Laemmli sample buffer. The samples were resolved by SDS-PAGE, transferred to nitrocellulose membrane, and blocked in 5% nonfat dried milk for 30 min. The membranes were incubated with primary antibodies for 1 h at RT or overnight at 4°C, followed by incubation with peroxidase-conjugated secondary antibodies for 1 h at RT. Immunoreactive bands were detected using an ECL-plus kit (Roche).

Immunofluorescence

For double staining of actin with the antibodies against p34, cortactin, or T-fimbrin and of actin with α-actinin– or fascin-GFP (HCT116), cells were preextracted for 30 s (0.5% Triton X-100 and 4% PEG in PEM buffer [100 mM Pipes, pH 6.9, 1 mM $MgCl_2$, and 1 mM EGTA]) to remove the cytoplasmic pool of the proteins, washed with PEM buffer, and then fixed with 4% paraformaldehyde for 20 min and stained. For detection of myosinX-, mDia2-, T-fimbrin–, VASP-, and fascin-GFP, cells were fixed and simultaneously extracted for 3 min in 4% paraformaldehyde and 0.5% Triton X-100 in PEM buffer, followed by 15-min fixation in 4% paraformaldehyde in PEM buffer. For all other stainings except for detection of endogenous fascin, cells were first fixed and then extracted for 1 min before staining. For fascin staining, cells were fixed in −20°C cold methanol for 6 min, postfixed with 4% paraformaldehyde for 20 min, and stained with an antifascin antibody.

BM preparation

BMs were prepared as previously described (Witz et al., 2001; Hotary et al., 2006). The peritoneal BM was isolated by stripping the overlying mesothelial cells from the rat mesentery using 0.5 N ammonium hydroxide and mounting the isolated mesentery on 6.5-mm-diameter Transwell (BD) from which the polycarbonate membrane was cut out. Thus, in this experiment, the BM still lies on its original stroma. 10^5 tumor cells were plated on the top of the BMs in DME supplemented with 15% FCS. DME supplemented with 15% FCS and 40 ng/ml HGF (Millipore) was used as a chemoattractant in the lower chamber. After 1–4 d of culture at 37°C, the samples were washed with PBS, fixed with 4% paraformaldehyde, and stained on both sides according to the protocol described in Immunofluorescence. Then, the membrane was cut out of the inserts and mounted. Cells were imaged

Table I. **siRNAs used in this study**

siRNA	Sequence (sense)	Concen.
		*n*M
si-control		30
si-fascin-1	5′-CAAAGACUCCACAGGCAAAUU-3′	30
si-fascin-2	5′-GAGCAUGGCUUCAUCGGCU-3′	30
si–T-fimbrin–1	5′-GAAAGAACCUUCCGUAACU-3′	30
si–T-fimbrin–2	5′-CTGAAAAUUUGCCGAAGUA-3′	30
si-myosinX-1	5′-CGUCGUAGCUGAUGUCUUA-3′	10
si-myosinX-2	5′-GGAGGAAAUUUCAGGGAAU-3′	10
si-p34	5′-CCAUGUAUGUUGAGUCUAA-3′ 5′-GCUCUAAGGCCUAUAUUCA-3′ 5′-GGACAGAGUCACAGUAGUC-3′ 5′-GUACGGGAGUUUCUUGGUA-3′	10
si-mDia2-1	5′-GAUGACAGAUGUGGUUAAA-3′	30
si-mDia2-2	5′-GAGUGUGUAUCCCAGAUUG-3′	30
si-vimentin-1	5′-GAGGGAAACUAAUCUGGAU-3′	2× 20
si-vimentin-2	5′-GGAAAUGGCUCGUCACCUU-3′	

Concen., concentration. Thermo Fisher Scientific did not provide the sequence of si-control.

with a 63× objective of a laser-scanning confocal microscope (LSM 510 META; Carl Zeiss, Inc.). The images and z sections were processed with ImageJ (National Institutes of Health) and Photoshop CS6 (Adobe).

For the time scale experiment, ∼30–40 cells were analyzed for each time point. A cell was considered in stage 2 or 3 if at least one of its protrusions was in the respective stage.

Knockdown experiments were performed in tri- or quadruplicates in two separate experiments. The length of each protrusion was calculated with Image Browser software (Carl Zeiss, Inc.) based on phalloidin staining. Approximately 80–120 protrusions were analyzed per experiment. Statistical analyses were performed with SigmaStat 3.0 software (Aspire Software International). Kruskal-Wallis one-way analysis of variance on ranks was used, and differences between the groups were considered significant if the p-value was <0.001. Multiple comparisons versus si-control cells were performed by the Dunn's method with an overall significance level of 0.05.

Gelatin degradation assay

FITC-labeled gelatin was obtained from Invitrogen. Alexa Fluor 350–conjugated gelatin was prepared by labeling porcine gelatin with Alexa Fluor 350 (Invitrogen) according to the manufacturer's instructions. Coverslips coated with fluorescent gelatin were prepared as described previously (Artym et al., 2006, 2009). In brief, coverslips (18 mm diameter) were coated with 0.5 µg/ml poly-L-lysine for 20 min at RT, washed with PBS, and cross-linked with 0.5% glutaraldehyde (Sigma-Aldrich) for 15 min. After three washes, the coverslips were inverted on an 80-µl drop of 0.2% fluorescently labeled gelatin in 2% sucrose in PBS and incubated for 10 min at RT. After washing with PBS, coverslips were incubated in 5 mg/ml sodium borohydride for 3 min, washed three times in PBS, and incubated in 2 ml of complete medium before adding the cells. To assess the ability of MDA-MB-231 cells to form invadopodia and degrade the matrix, 7×10^4 cells were plated on fluorescent gelatin–coated coverslips and incubated at 37°C for 5.5 h.

Knockdown experiments were performed in duplicate at least three times. Cells were imaged with a 63× objective of a wide-field microscope (DM6000 B/M; Leica) equipped with a charge-coupled device camera (CoolSNAP HQ; Photometrics). To quantify the number of cells able to degrade the gelatin, ∼100 cells per duplicate were randomly chosen: a cell was considered a degrading cell if areas of degraded matrix (dark holes in the bright fluorescent gelatin) were present below the cell. To quantify the extent of the matrix degradation, the total degraded area was measured using MetaMorph 7.2.6 (MDS Analytical Technologies). The outside of each cell that degraded the gelatin was first delimited to calculate the total cell surface. The fluorescent intensity of the gelatin around each cell was measured. We excluded the shallow degradation spots that were probably a consequence of diffuse action of MMPs along the ventral surface of cells. Indeed, we postulated that they do not correspond to a focal accumulation of MMPs and should not be considered a result of invadopodia activity. Thus, the threshold command of MetaMorph was used to detect the pixels of intensity lower than half of the gelatin fluorescent intensity, thus taking into account only the deep degradation foci. The degradation index was calculated as the total area of those degradation spots per cell normalized to the total surface of this cell. Statistical analyses were performed with SigmaStat 3.0 software. Kruskal-Wallis one-way analysis of variance on ranks was used, and differences between the groups were considered significant if the p-value was <0.001. Multiple comparisons versus si-control cells were checked by the Holm-Sidak method with an overall significance level of 0.05.

Invadopodia lifetime analysis

MDA-MB-231 cells expressing mCherry-LifeAct were treated with the following siRNA: si-control, si-p34, si-fascin-2, or si-myosinX-2. After 72 h of transfection, cells were plated on FITC-gelatin–coated coverslips and allowed to adhere for 3 h. The coverslips were then mounted in a Ludin Chamber (Life Imaging Services) with L15 medium without phenol red (Invitrogen) supplemented with 15% FBS and placed in a 37°C heated chamber. Images were collected with the 63× objective of an inverted microscope (TE2000-U; Nikon) equipped with a spinning disk head (CSU22; Yokogawa) and a charge-coupled device camera (CoolSNAP HQ2; Photometrics) and operated with MetaMorph 7.1.4 (MDS Analytical Technologies). 15 random fields were chosen, and fluorescence images were taken every 2 min for mCherry-LifeAct and every 30 min for FITC-gelatin during 5–6 h. Accumulation of actin (visualized by mCherry-LifeAct) in a degradation spot defined an invadopodium. Invadopodia lifetimes were then analyzed by counting the time lapsed between the first and last frames in which an individual invadopodium was observed. For each lifetime, measurements were made on a total of ∼150 invadopodia in 30–40 individual cells from at least three separate experiments. Statistical analyses were performed with SigmaStat 3.0 software. Kruskal-Wallis one-way analysis of variance on ranks was used, and differences between the groups were considered significant if the p-value was <0.001. Multiple comparisons versus si-control cells were checked by the Dunn's method with an overall significance level of 0.05.

Chemoinvasion assay

Matrigel was purchased from BD. Laminin (Invitrogen) was labeled with Alexa Fluor 488 with a protein labeling kit (Invitrogen) according to the manufacturer's instructions.

Transwell inserts with a 10.5-mm-diameter membrane covered with 1-µm-diameter pores (BD) were coated with 80 µl with a 1:1 mix of 9–10 mg/ml Matrigel with 0.5 mg/ml of labeled or unlabeled laminin for 1 h at 4°C. 75 µl was then removed, and the inserts were put at 37°C for 30 min to allow polymerization of the Matrigel. Complete medium was added in both sides of the inserts to rehydrate the matrix before adding the cells. 4×10^4 MDA-MB-231 cells or 5×10^4 HCT116 cells were resuspended in 1 ml DME and added to the upper side of the filters. DME supplemented with 15% FCS and 40 ng/ml HGF was used as a chemoattractant. After 15-h incubation at 37°C, cells were washed with PBS and fixed with 4% paraformaldehyde. For immunostaining, the membrane was cut out of the inserts and stained from both sides according to the protocol described in Immunofluorescence. Cells were imaged with a 63× objective of an LSM 510 META laser-scanning confocal microscope. The images and z sections were processed with ImageJ and Photoshop CS6. Knockdown experiments were performed in duplicates at least three times. The length of each protrusion was calculated with Image Browser software based on phalloidin staining. Approximately 150 protrusions were analyzed per duplicate and per experiment. For each experiment, protrusions were classified into two groups according to their length: short (<5 µm) and long protrusions (>5 µm). The mean repartition between all experiments was then calculated. Statistical analyses were performed with SigmaStat 3.0 software. Kruskal-Wallis one-way analysis of variance on ranks was used, and differences between the groups were considered significant if the p-value was <0.001. Multiple comparisons versus si-control cells were checked by the Holm-Sidak method with an overall significance level of 0.05.

EM

For EM experiments, cell density was increased to 2×10^5 cells per insert (1-µm pore filters). All chemical components were purchased from Electron Microscopy Sciences. Cells were fixed for at least 2 h in 2% glutaraldehyde in cacodylate acid, pre- or postextracted for 30 s in the extraction buffer with 1% Triton X-100, and postfixed for 20 min with 1 mg/ml tannic acid in H_2O. Cells were stained with 0.2% osmium in H_2O for 20 min on ice and 20 min with 2 mg/ml uranyl acid in H_2O. To detect cells in semithin

sections, cells were colored with 0.6% toluidine blue. Membranes were then progressively dehydrated in ethanol, poststained for 20 min with 2 mg/ml uranyl acid in 100% ethanol, and then washed in 100% ethanol and embedded in epon (Araldite502/Embed-812 embedding media; Electron Microscopy Sciences) according to the manufacturer's recommendations. Blocks were cut as ultrathin longitudinal sections and put on 100-mesh grids coated with 0.8% Formvar. Samples were contrasted with a solution of lead-citrate, rinsed with H_2O, and observed with a transmission electron microscope (Philips CM120; FEI Company).

Online supplemental material

Fig. S1 shows that lamellipodial and filopodial markers are present in invadopodia. Fig. S2 shows the spatial distribution of lamellipodial and filopodial markers in mature invadopodia. Fig. S3 shows the frequency of localization of lamellipodial and filopodial markers and their role in mature invadopodia. Fig. S4 shows additional electron micrographs of mature invadopodia. Fig. S5 shows localization and a role of microtubules and vimentin in mature invadopodia. Videos 1 and 2 show F-actin dynamics in MDA-MB-231 cells plated on fluorescent gelatin and treated with control or p34 siRNA, respectively. Online supplemental material is available at http://www.jcb.org/cgi/content/full/jcb.200909113/DC1.

We are grateful to S. Weiss and F. Sabeh for teaching M. Schoumacher the isolation of native BM. We thank P. Chavrier and G. Le-Dez for help with the gelatin degradation assay and G. Raposo's laboratory for help with EM. We also thank R. Cheney and P. Chavrier for gifts of reagents and G. Montagnac, S. Duffy, P. Chavrier, and T. Svitkina for critical reading of the manuscript. The authors greatly acknowledge F. Waharte of the PICT-IBiSA Imaging Facility.

This work was supported by grants from Agence Nationale de Recherche (ANR-09-JCJC0023-01) and Equipe Labellisée LIGUE 2008 to D.M. Vignjevic and a Ministère de la Recherche and European Molecular Biology Organization short-term fellowship to M. Schoumacher.

Submitted: 18 September 2009
Accepted: 5 April 2010

References

Alberts, A.S. 2001. Identification of a carboxyl-terminal diaphanous-related formin homology protein autoregulatory domain. *J. Biol. Chem.* 276:2824–2830. doi:10.1074/jbc.M006205200

Arpin, M., E. Friederich, M. Algrain, F. Vernel, and D. Louvard. 1994. Functional differences between L- and T-plastin isoforms. *J. Cell Biol.* 127:1995–2008. doi:10.1083/jcb.127.6.1995

Artym, V.V., Y. Zhang, F. Seillier-Moiseiwitsch, K.M. Yamada, and S.C. Mueller. 2006. Dynamic interactions of cortactin and membrane type 1 matrix metalloproteinase at invadopodia: defining the stages of invadopodia formation and function. *Cancer Res.* 66:3034–3043. doi:10.1158/0008-5472.CAN-05-2177

Artym, V.V., K.M. Yamada, and S.C. Mueller. 2009. ECM degradation assays for analyzing local cell invasion. *Methods Mol. Biol.* 522:211–219.

Ayala, I., M. Baldassarre, G. Giacchetti, G. Caldieri, S. Tetè, A. Luini, and R. Buccione. 2008. Multiple regulatory inputs converge on cortactin to control invadopodia biogenesis and extracellular matrix degradation. *J. Cell Sci.* 121:369–378. doi:10.1242/jcs.008037

Baldassarre, M., I. Ayala, G. Beznoussenko, G. Giacchetti, L.M. Machesky, A. Luini, and R. Buccione. 2006. Actin dynamics at sites of extracellular matrix degradation. *Eur. J. Cell Biol.* 85:1217–1231. doi:10.1016/j.ejcb.2006.08.003

Bear, J.E., T.M. Svitkina, M. Krause, D.A. Schafer, J.J. Loureiro, G.A. Strasser, I.V. Maly, O.Y. Chaga, J.A. Cooper, G.G. Borisy, and F.B. Gertler. 2002. Antagonism between Ena/VASP proteins and actin filament capping regulates fibroblast motility. *Cell*. 109:509–521. doi:10.1016/S0092-8674(02)00731-6

Bohil, A.B., B.W. Robertson, and R.E. Cheney. 2006. Myosin-X is a molecular motor that functions in filopodia formation. *Proc. Natl. Acad. Sci. USA*. 103:12411–12416. doi:10.1073/pnas.0602443103

Bowden, E.T., M. Barth, D. Thomas, R.I. Glazer, and S.C. Mueller. 1999. An invasion-related complex of cortactin, paxillin and PKCmu associates with invadopodia at sites of extracellular matrix degradation. *Oncogene*. 18:4440–4449. doi:10.1038/sj.onc.1202827

Bowden, E.T., E. Onikoyi, R. Slack, A. Myoui, T. Yoneda, K.M. Yamada, and S.C. Mueller. 2006. Co-localization of cortactin and phosphotyrosine identifies active invadopodia in human breast cancer cells. *Exp. Cell Res.* 312:1240–1253. doi:10.1016/j.yexcr.2005.12.012

Buccione, R., J.D. Orth, and M.A. McNiven. 2004. Foot and mouth: podosomes, invadopodia and circular dorsal ruffles. *Nat. Rev. Mol. Cell Biol.* 5:647–657. doi:10.1038/nrm1436

Chen, W.T. 1989. Proteolytic activity of specialized surface protrusions formed at rosette contact sites of transformed cells. *J. Exp. Zool.* 251:167–185. doi:10.1002/jez.1402510206

Clark, E.S., A.S. Whigham, W.G. Yarbrough, and A.M. Weaver. 2007. Cortactin is an essential regulator of matrix metalloproteinase secretion and extracellular matrix degradation in invadopodia. *Cancer Res.* 67:4227–4235. doi:10.1158/0008-5472.CAN-06-3928

Correia, I., D. Chu, Y.H. Chou, R.D. Goldman, and P. Matsudaira. 1999. Integrating the actin and vimentin cytoskeletons. Adhesion-dependent formation of fimbrin-vimentin complexes in macrophages. *J. Cell Biol.* 146:831–842. doi:10.1083/jcb.146.4.831

Gupton, S.L., and F.B. Gertler. 2007. Filopodia: the fingers that do the walking. *Sci. STKE*. 2007:re5. doi:10.1126/stke.4002007re5

Hashimoto, Y., M. Skacel, and J.C. Adams. 2005. Roles of fascin in human carcinoma motility and signaling: prospects for a novel biomarker? *Int. J. Biochem. Cell Biol.* 37:1787–1804. doi:10.1016/j.biocel.2005.05.004

Higgs, H.N., and T.D. Pollard. 2001. Regulation of actin filament network formation through ARP2/3 complex: activation by a diverse array of proteins. *Annu. Rev. Biochem.* 70:649–676. doi:10.1146/annurev.biochem.70.1.649

Hotary, K., X.Y. Li, E. Allen, S.L. Stevens, and S.J. Weiss. 2006. A cancer cell metalloprotease triad regulates the basement membrane transmigration program. *Genes Dev.* 20:2673–2686. doi:10.1101/gad.1451806

Hung, W., and B. Elliott. 2001. Co-operative effect of c-Src tyrosine kinase and Stat3 in activation of hepatocyte growth factor expression in mammary carcinoma cells. *J. Biol. Chem.* 276:12395–12403. doi:10.1074/jbc.M010715200

Kikuchi, K., and K. Takahashi. 2008. WAVE2- and microtubule-dependent formation of long protrusions and invasion of cancer cells cultured on three-dimensional extracellular matrices. *Cancer Sci.* 99:2252–2259. doi:10.1111/j.1349-7006.2008.00927.x

Koestler, S.A., S. Auinger, M. Vinzenz, K. Rottner, and J.V. Small. 2008. Differentially oriented populations of actin filaments generated in lamellipodia collaborate in pushing and pausing at the cell front. *Nat. Cell Biol.* 10:306–313. doi:10.1038/ncb1692

Kopp, P., R. Lammers, M. Aepfelbacher, G. Woehlke, T. Rudel, N. Machuy, W. Steffen, and S. Linder. 2006. The kinesin KIF1C and microtubule plus ends regulate podosome dynamics in macrophages. *Mol. Biol. Cell*. 17:2811–2823. doi:10.1091/mbc.E05-11-1010

Kreis, T.E. 1987. Microtubules containing detyrosinated tubulin are less dynamic. *EMBO J.* 6:2597–2606.

Kural, C., A.S. Serpinskaya, Y.H. Chou, R.D. Goldman, V.I. Gelfand, and P.R. Selvin. 2007. Tracking melanosomes inside a cell to study molecular motors and their interaction. *Proc. Natl. Acad. Sci. USA*. 104:5378–5382. doi:10.1073/pnas.0700145104

Linder, S. 2007. The matrix corroded: podosomes and invadopodia in extracellular matrix degradation. *Trends Cell Biol.* 17:107–117. doi:10.1016/j.tcb.2007.01.002

Lizárraga, F., R. Poincloux, M. Romao, G. Montagnac, G. Le Dez, I. Bonne, G. Rigaill, G. Raposo, and P. Chavrier. 2009. Diaphanous-related formins are required for invadopodia formation and invasion of breast tumor cells. *Cancer Res.* 69:2792–2800. doi:10.1158/0008-5472.CAN-08-3709

Lorenz, M., H. Yamaguchi, Y. Wang, R.H. Singer, and J. Condeelis. 2004. Imaging sites of N-wasp activity in lamellipodia and invadopodia of carcinoma cells. *Curr. Biol.* 14:697–703. doi:10.1016/j.cub.2004.04.008

Mattila, P.K., and P. Lappalainen. 2008. Filopodia: molecular architecture and cellular functions. *Nat. Rev. Mol. Cell Biol.* 9:446–454. doi:10.1038/nrm2406

Maupin, P., and T.D. Pollard. 1983. Improved preservation and staining of HeLa cell actin filaments, clathrin-coated membranes, and other cytoplasmic structures by tannic acid-glutaraldehyde-saponin fixation. *J. Cell Biol.* 96:51–62. doi:10.1083/jcb.96.1.51

Mendez, M.G., S.I. Kojima, and R.D. Goldman. 2010. Vimentin induces changes in cell shape, motility, and adhesion during the epithelial to mesenchymal transition. *FASEB J.* doi:10.1096/fj.09-151639

Nakahara, H., L. Howard, E.W. Thompson, H. Sato, M. Seiki, Y. Yeh, and W.T. Chen. 1997. Transmembrane/cytoplasmic domain-mediated membrane type 1-matrix metalloprotease docking to invadopodia is required for cell invasion. *Proc. Natl. Acad. Sci. USA*. 94:7959–7964. doi:10.1073/pnas.94.15.7959

Oser, M., H. Yamaguchi, C.C. Mader, J.J. Bravo-Cordero, M. Arias, X. Chen, V. Desmarais, J. van Rheenen, A.J. Koleske, and J. Condeelis. 2009. Cortactin regulates cofilin and N-WASp activities to control the stages

of invadopodium assembly and maturation. *J. Cell Biol.* 186:571–587. doi:10.1083/jcb.200812176

Philippar, U., E.T. Roussos, M. Oser, H. Yamaguchi, H.D. Kim, S. Giampieri, Y. Wang, S. Goswami, J.B. Wyckoff, D.A. Lauffenburger, et al. 2008. A Mena invasion isoform potentiates EGF-induced carcinoma cell invasion and metastasis. *Dev. Cell*. 15:813–828. doi:10.1016/j.devcel .2008.09.003

Pi, X., R. Ren, R. Kelley, C. Zhang, M. Moser, A.B. Bohil, M. Divito, R.E. Cheney, and C. Patterson. 2007. Sequential roles for myosin-X in BMP6-dependent filopodial extension, migration, and activation of BMP receptors. *J. Cell Biol.* 179:1569–1582. doi:10.1083/jcb.200704010

Poincloux, R., F. Lizárraga, and P. Chavrier. 2009. Matrix invasion by tumour cells: a focus on MT1-MMP trafficking to invadopodia. *J. Cell Sci.* 122:3015–3024. doi:10.1242/jcs.034561

Sakurai-Yageta, M., C. Recchi, G. Le Dez, J.B. Sibarita, L. Daviet, J. Camonis, C. D'Souza-Schorey, and P. Chavrier. 2008. The interaction of IQGAP1 with the exocyst complex is required for tumor cell invasion downstream of Cdc42 and RhoA. *J. Cell Biol.* 181:985–998. doi:10.1083/jcb.200709076

Schnaeker, E.M., R. Ossig, T. Ludwig, R. Dreier, H. Oberleithner, M. Wilhelmi, and S.W. Schneider. 2004. Microtubule-dependent matrix metalloproteinase-2/matrix metalloproteinase-9 exocytosis: prerequisite in human melanoma cell invasion. *Cancer Res.* 64:8924–8931. doi:10.1158/0008-5472.CAN-04-0324

Sousa, A.D., and R.E. Cheney. 2005. Myosin-X: a molecular motor at the cell's fingertips. *Trends Cell Biol.* 15:533–539. doi:10.1016/j.tcb.2005 .08.006

Svitkina, T.M., and G.G. Borisy. 1999. Arp2/3 complex and actin depolymerizing factor/cofilin in dendritic organization and treadmilling of actin filament array in lamellipodia. *J. Cell Biol.* 145:1009–1026. doi:10.1083/jcb.145.5.1009

Svitkina, T.M., E.A. Bulanova, O.Y. Chaga, D.M. Vignjevic, S. Kojima, J.M. Vasiliev, and G.G. Borisy. 2003. Mechanism of filopodia initiation by reorganization of a dendritic network. *J. Cell Biol.* 160:409–421. doi:10.1083/jcb.200210174

Thiery, J.P. 2002. Epithelial-mesenchymal transitions in tumour progression. *Nat. Rev. Cancer*. 2:442–454. doi:10.1038/nrc822

Tokuo, H., and M. Ikebe. 2004. Myosin X transports Mena/VASP to the tip of filopodia. *Biochem. Biophys. Res. Commun.* 319:214–220. doi:10.1016/j.bbrc.2004.04.167

Trichet, L., C. Sykes, and J. Plastino. 2008. Relaxing the actin cytoskeleton for adhesion and movement with Ena/VASP. *J. Cell Biol.* 181:19–25. doi:10.1083/jcb.200710168

Vignjevic, D., and G. Montagnac. 2008. Reorganisation of the dendritic actin network during cancer cell migration and invasion. *Semin. Cancer Biol.* 18:12–22. doi:10.1016/j.semcancer.2007.08.001

Vignjevic, D., S. Kojima, Y. Aratyn, O. Danciu, T. Svitkina, and G.G. Borisy. 2006. Role of fascin in filopodial protrusion. *J. Cell Biol.* 174:863–875. doi:10.1083/jcb.200603013

Vignjevic, D., M. Schoumacher, N. Gavert, K.P. Janssen, G. Jih, M. Laé, D. Louvard, A. Ben-Ze'ev, and S. Robine. 2007. Fascin, a novel target of beta-catenin-TCF signaling, is expressed at the invasive front of human colon cancer. *Cancer Res.* 67:6844–6853. doi:10.1158/0008-5472.CAN-07-0929

Wear, M.A., and J.A. Cooper. 2004. Capping protein: new insights into mechanism and regulation. *Trends Biochem. Sci.* 29:418–428. doi:10.1016/j.tibs.2004.06.003

Weaver, A.M. 2006. Invadopodia: specialized cell structures for cancer invasion. *Clin. Exp. Metastasis*. 23:97–105. doi:10.1007/s10585-006-9014-1

Weaver, A.M. 2008. Invadopodia. *Curr. Biol.* 18:R362–R364. doi:10.1016/j.cub.2008.02.028

Weaver, A.M., A.V. Karginov, A.W. Kinley, S.A. Weed, Y. Li, J.T. Parsons, and J.A. Cooper. 2001. Cortactin promotes and stabilizes Arp2/3-induced actin filament network formation. *Curr. Biol.* 11:370–374. doi:10.1016/S0960-9822(01)00098-7

Witz, C.A., I.A. Montoya-Rodriguez, S. Cho, V.E. Centonze, L.F. Bonewald, and R.S. Schenken. 2001. Composition of the extracellular matrix of the peritoneum. *J. Soc. Gynecol. Investig.* 8:299–304. doi:10.1016/S1071-5576(01)00122-8

Yamaguchi, H., M. Lorenz, S. Kempiak, C. Sarmiento, S. Coniglio, M. Symons, J. Segall, R. Eddy, H. Miki, T. Takenawa, and J. Condeelis. 2005. Molecular mechanisms of invadopodium formation: the role of the N-WASP–Arp2/3 complex pathway and cofilin. *J. Cell Biol.* 168:441–452. doi:10.1083/jcb.200407076

Yang, C., L. Czech, S. Gerboth, S. Kojima, G. Scita, and T. Svitkina. 2007. Novel roles of formin mDia2 in lamellipodia and filopodia formation in motile cells. *PLoS Biol.* 5:e317. doi:10.1371/journal.pbio.0050317

Yilmaz, M., and G. Christofori. 2009. EMT, the cytoskeleton, and cancer cell invasion. *Cancer Metastasis Rev.* 28:15–33. doi:10.1007/s10555-008-9169-0

Zhao, Y., Q. Yan, X. Long, X. Chen, and Y. Wang. 2008. Vimentin affects the mobility and invasiveness of prostate cancer cells. *Cell Biochem. Funct.* 26:571–577. doi:10.1002/cbf.1478